BOOKLET FOR FEL DESIGN:

A Collection of Practical Formulae

Giuseppe Dattoli

ENEA – Centro Ricerche Energia Frascati, Via Enrico Fermi 45,
Frascati, Rome, Italy

Pier Luigi Ottaviani, Simonetta Pagnutti

ENEA – Centro Ricerche Energia Bologna, Via Don Fiammelli, 2
Bologna, Italy

BOOKLET FOR FEL DESIGN: A COLLECTION OF PRACTICAL FORMULAE.

G. DATTOLI, P. L. OTTAVIANI and S. PAGNUTTI

PREFACE

This booklet is just a collection of formulae for the design of a FEL device and a "quick" evaluation of its performance.
These formulae, developed over the last thirty years, have been the workhorses allowing a substantive assistance in understanding the FEL Physics. They have provided us with a concrete tool for analysis when more serious and complete computations were not available or demanded long computational times.
We decided to present this synopsis for various reasons, some of which are listed below:

a) Over the years we contributed to most of the formulae typically exploited in the analysis of FEL devices

b) We have been involved in the design and the construction of different types of FEL, ranging from Storage Ring to Self Amplified Spontaneous Emission (SASE) devices. We can therefore confirm the usefulness of these formulae as a design tool

c) we are often contacted by young researchers (and not only) asking for help in finding empirical formulae on gain, saturation…which they heard about, but have found difficult to locate in the vast amount of FEL literature

d) these formulae are often rediscovered and they are not always used correctly.

The above reasons compelled us to collect the formulae which are in our notes often consulted in our daily work.
We have reduced the discussion to a minimum and, indeed, we report the formulae and their range of validity without great detailed explanation.
It will also be evident that we are essentially referring to "home-made" work and that we do not refer to other contributions, except for the Ming Xie formula, which played a significant role in the development of high gain FEL devices.
As already remarked, the booklet summarizes about thirty years of work in the field, and we owe our gratitude to an almost infinite number of colleagues, who helped us indirectly contributing to the work or giving their criticisms. It is therefore quite impossible to make a complete list, notwithstanding we have the pleasure of recognizing:

W. B. Colson - his clear and careful work has strongly influenced our researches,

Our Friends and Younger co-workers **L. Giannessi, M. Migliorati, A. Renieri, E. Sabia, A. Segreto**,

and finally it is a pleasure to thank **S. G. Biedron and H. P. Freund** for suggestions during the early stages of the work.

We have forgotten many others, this is our fault only and we sincerely apologize.

CONTENTS

1 – GENERALITIES ON FEL AND DEFINITIONS

1.1 Physical constants used in the practical formulae[1]

$m_e = 9.109382 \cdot 10^{-31} kg$

$c = 2.99792458 \cdot 10^{8} ms^{-1}$

$e = 1.60217646 \cdot 10^{-19} C$

$1eV = 1.60217646 \cdot 10^{-12} erg$

$m_e c^2 = 0.5109989 MeV$

$Z_0 (free\ space\ impedence) = \mu_0 c = 376.7303 \Omega$

The notation $L[m]$ denotes a length given in meters, $I\left[\frac{MW}{cm^2}\right]$ denotes an intensity given in megawatts per square centimetres and so on.

1.2 1-D equations and parameters

The dynamic of the system of an e-beam travelling in an undulator, along the longitudinal z-direction (see Fig.1 for axes orientation), interacting with a plane e.m. wave is specified by the Lorentz's equations of motion (Gaussian system)

$$m_e \frac{d}{dt}(\gamma \vec{v}) = -e\left(\vec{E}_s + \frac{1}{c}\vec{v} \times \vec{B}\right)$$

$$\frac{d}{dt}\gamma = -\frac{e}{m_e c^2}\vec{E}_s \cdot \vec{v}$$

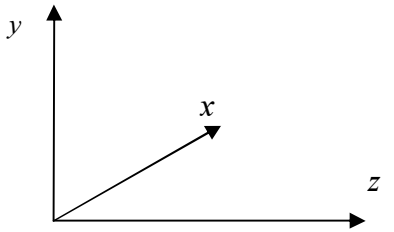

Fig. 1.1. Axes orientation

where

$\vec{v}$ *electron velocity*

$\gamma = \frac{E}{m_e c^2}$ *electron relativistic factor*, *E electron energy*

$\vec{B} = \vec{B}_s + \vec{B}_u$

$\vec{B}_u \equiv [0,\ B_0 \sin(k_u z),\ 0]$

$\vec{E}_s \equiv [E_s \cos\psi_s,\ 0,\ 0]$ linearly polarized undulator

$\vec{B}_s \equiv [0,\ E_s \cos\psi_s,\ 0]$

[1] European Physical Journal C 15, n. 1-4 (2000)

$\vec{B}_u \equiv [B_0\, cos(k_u z),\, B_0\, sin(k_u z),\, 0]$

$\vec{E}_s \equiv [E_s \cos\psi_s,\, -E_s \sin\psi_s,\, 0]$ helically polarized undulator

$\vec{B}_s \equiv [E_s \sin\psi_s,\, E_s \cos\psi_s,\, 0]$

$\psi_s = k_s z - \omega\, t + \phi_s$

$\lambda_s\,, \quad k_s = \dfrac{2\pi}{\lambda_s}, \quad \omega = ck_s$ *laser field wave length, wave number and frequency*

$\lambda_u\,, \quad k_u = \dfrac{2\pi}{\lambda_u}$ *undulator period and wave number*

$N\,, \quad L = N\lambda_u$ *number of undulator periods and undulator length*

Halbach configuration undulator parameters :

$$B_0 = 2B_r \frac{\sin\left(\dfrac{\pi}{M}\right)}{\dfrac{\pi}{M}}\left[1-\exp\left(-\frac{2\pi h}{\lambda_u}\right)\right]\exp\left(-\frac{\pi g}{\lambda_u}\right)$$

M *number of blocks per period*

h *magnet height*

g *gap*

B_r *remanent field*

1.3 FEL equations

The evolution of electrons and electric field is described by the coupled equations (averaged over an undulator period)

$$\frac{d\gamma}{dz} = \frac{K^*}{\gamma} e_s f_b \cos\psi$$

$$\frac{d\zeta}{dz} = k_u - \frac{k_u + k_s}{2\gamma^2}\left[1 + K^{*2} + \left(\frac{e_s}{k_s}\right)^2 - 2K^* \frac{e_s}{k_s} f_b \sin\psi\right]$$

$$\frac{de_s}{dz} = -2\pi \frac{e}{m_e c^3} |J| K^* f_b \left\langle \frac{\cos\psi}{\gamma} \right\rangle$$

$$e_s \frac{d\phi_s}{dz} = 2\pi \frac{e}{m_e c^3} |J| \left[K^* f_b \left\langle \frac{\sin\psi}{\gamma} \right\rangle - \frac{e_s}{k_s} \left\langle \frac{1}{\gamma} \right\rangle \right]$$

where

$\psi = \zeta + \phi_s$

$\zeta = (k_u + k_s)\int_0^t \bar{v}_z(t')dt' - \omega t$ *dimensionless electron phase*

$\bar{v}_z$ *denotes average over the undulator period*

$\langle \quad \rangle$ *indicates average over electrons in a ψ period*

e_s *normalized electric field amplitude* $\left[l^{-1}\right]$

f_b *Bessel function factor*

$e_s = \dfrac{eE_s}{\sqrt{2}m_e c^2}$, $K^* = K/\sqrt{2}$, $f_b = J_0(\xi) - J_1(\xi)$ *linear undulator* (J_0,$_1$ *cylindrical Bessel function*)

$e_s = \dfrac{eE_s}{m_e c^2}$, $K^* = K$, $f_b = 1$ *helical undulator*

$K = \dfrac{eB_0\lambda_u}{2\pi m_e c^2}$ *undulator parameter*

$\xi = \dfrac{1}{2}K^{*2}\left(1 + K^{*2}\right)^{-1}$

J *electron beam current density*

1.4 Radiation parameters

$\lambda_0 = \dfrac{\lambda_u}{2\gamma^2}(1 + K^{*2})$, $\omega_0 = 2\pi c/\lambda_0$ *resonant wavelength and frequency (central emission)*

$\lambda_s = \lambda_0\left(1 - \nu/2\pi N\right)^{-1}$; $\nu = L\dfrac{d\varsigma}{dz} = 2\pi N\dfrac{\omega_0 - \omega}{\omega_0}$ *detuning parameter*

$f(\nu) = \left[sinc\left(\nu/2\right)\right]^2$ *spontaneous emission line shape*

$I = \dfrac{c}{4\pi}\left(\dfrac{m_e c^2}{e}\right)^2 e_s{}^2$ *intensity*

An approximation of the line shape useful to evaluate inhomogeneous broadening effects is (see Appendix A)

$f(\nu) \cong exp\left(-\alpha\nu^2\right)cos(\beta\nu)$

$\alpha = 0.04464$, $\beta = 0.2823$ *for* $-4 \le \nu \le 4$ $\left(relative\ error < 1\%\right)$

1.5 Correspondence between Gaussian, MKS and practical units

$\dfrac{e}{m_e c^3}(gaussian) \rightarrow \dfrac{Z_0 c}{4\pi}\dfrac{e}{m_e c^3}(MKS) = \dfrac{e}{m_e c}10^{-7}\left[A^{-1}\right] = I_0^{-1}$

$I_o = \dfrac{4\pi}{Z_0 c}\dfrac{m_e c^3}{e} = 1.704509 \cdot 10^4\ A$ *Alfvèn current*

$I\left[\dfrac{MW}{cm^2}\right] = \dfrac{10^{-3}}{4\pi c}\left(\dfrac{m_e c^2}{e}\right)^2\left(e_s\left[m^{-1}\right]\right)^2 = 6.931215 \cdot 10^{-2}\left(e_s\left[m^{-1}\right]\right)^2$

$K = \dfrac{eB_0\lambda_u}{2\pi m_e c^2} = \dfrac{\lambda_u[cm]B_0[KG]}{10.71}$

1.6 Betatron motion in an undulator focusing in both transverse directions

$$\frac{d^2}{dz^2}(x_0, y_0) = -k_\beta^2 (x_0, y_0)$$

$$k_\beta = \frac{K^* k_u}{\sqrt{2}\,\gamma} \qquad \textit{betatron motion wave number}$$

1.7 e-beam energy distribution

$$\Phi(\varepsilon) = \frac{1}{\sqrt{2\pi}\sigma_\varepsilon} exp\left(-\frac{\varepsilon^2}{2\sigma_\varepsilon^2}\right) \quad \textit{relative energy distribution}$$

$\varepsilon = \dfrac{\gamma - \gamma_0}{\gamma_0}$, σ_ε *relative energy and energy spread*

$\mu_\varepsilon = 4N\sigma_\varepsilon$ *energy distribution inhomogeneous broadening parameter*

1.8 e-beam phase space distribution

no coupling between x, y planes

$F(x, x', y, y') = W(x, x')W(y, y')$ *distribution function*

$$W(\eta, \eta') = \frac{1}{2\pi\varepsilon_\eta} exp\left[-\frac{1}{2\varepsilon_\eta}\left(\beta_\eta \eta'^2 + 2\alpha_\eta \eta\eta' + \gamma_\eta \eta^2\right)\right]$$

ε_η *emittance in the* (η, η') *plane*

$\alpha_\eta, \beta_\eta, \gamma_\eta$ *Twiss coefficients with* $\beta_\eta \gamma_\eta - \alpha_\eta^2 = 1$

$$\mu_{\eta'} = \frac{4N\gamma^2\varepsilon_\eta}{\left(1 + K^{*2}\right)\beta_\eta}, \qquad \mu_\eta = \frac{4N\gamma^2\varepsilon_\eta}{\left(1 + K^{*2}\right)\gamma_\eta} k_\beta^2$$

k_β *betatron motion wave number*

$\mu_\eta, \mu_{\eta'}$ *emittance inhomogeneous parameters*

1.9 Matched beam

$$\alpha_\eta = 0, \ \beta_\eta = k_\beta^{-1} \ \rightarrow \ \mu_\eta = \mu_{\eta'} = \sqrt{2}\,\frac{4NK^*}{1 + K^{*2}} \frac{A_{n,\eta}}{\lambda_u}$$

$A_{n,\eta} = \gamma\pi\varepsilon_\eta$ *normalized e – beam emittance*

1.10 Bazarov-Sinclair formula for optimized dc-gun photo-injectors

e-beam transverse normalized rms emittance ε_x vs bunch charge q and rms bunch length σ_z [2]

$$\varepsilon_x[mm\cdot mrad] = (0.73 + \frac{0.15}{(\sigma_z[mm])^{2.3}})\, q[nC]$$

1.11 e-beam optimized longitudinal rms emittance[3]

$$\varepsilon_z[keV\cdot mm] = a + b\,\sigma_z + c\,(\sigma_z)^d,$$

$$a = 9.1 + 49.8\,q + 32\,q^2,$$

$$b = 27.1 - 72.8\,q - 47\,e^{-3..3q},$$

$$c = -2.3 + 3.3q + 1.04\,q^{-1.02}$$

$$d = 1.91\frac{e^{8.52q}}{1+\frac{1.91}{5.57}(e^{8.52q}-1)} \qquad with\ q[nC],\ \sigma_z[mm]$$

1.12 Pendulum equations and Colson's dimensionless variables (see Appendix B)

$$\frac{d^2}{d\tau^2}\zeta = |a|\ cos(\zeta+\phi)$$

$$\frac{da}{d\tau} = -j\left\langle e^{-i\zeta}\right\rangle$$

$$\tau = \frac{z}{L}$$

a *dimensionless field Colson's amplitude*

$$|a| = \frac{k_s}{\gamma^4}K^*(N\lambda_u)^2\left(1+K^{*2}\right)f_b\,e_s = 4\pi\left(\frac{N}{\gamma}\right)^2 K^*\lambda_u\left(1-\frac{\nu}{2\pi N}\right)f_b\,e_s$$

$j = 2\pi\, g_0$ *Colson's dimensionless current*

$$g_0 = \frac{16\pi}{\gamma}\frac{|J|}{I_0}\lambda_0 L N^2 \xi\, f_b{}^2 \qquad small\ signal\ gain\ FEL\ coefficient$$

$$= 4\pi\frac{|J|}{I_0}\left(\frac{N}{\gamma}\right)^3\left(\lambda_u K^* f_b\right)^2$$

$$G = \frac{|a|^2 - |a_0|^2}{|a_0|^2} \qquad FEL-Gain,\ a_0 = seed\ Colson's\ amplitude$$

1.13 e-beam power and saturation intensity

[2] Formula derived by Bazarov and Sinclair, Phys. Rev. Special Topics, Acc. and Beams **8**, 034202 (2005).
[3]) Formula derived by the Authors using the Bazarov and Sinclair numerical data.

The FEL-saturation intensity[4] is defined as the field intensity halving the small signal gain and is implicitly contained in the definition of Colson's dimensionless intensity

$$I_S = \frac{c}{8\pi}\left(\frac{m_e c^2}{e}\right)^2 \left(\frac{\gamma}{N}\right)^4 \left(\lambda_u K^* f_b\right)^{-2} \qquad \textit{saturation intensity}$$

$$|a|^2 = 8\pi^2 \frac{I}{I_S}\left(1 - \frac{\nu}{2\pi N}\right)^2$$

$$P_E = E \cdot \frac{|J|}{e} = \frac{m_e c^2}{e}\gamma |J| = 2N g_0 I_S \qquad e-beam \;\; power \;\; density$$

$$I_S\left[\frac{MW}{cm^2}\right] = 6.9312 \cdot 10^2 \frac{1}{2}\left(\frac{\gamma}{N}\right)^4 \left(\lambda_u [cm] K^* f_b\right)^{-2}$$

$$P_E\left[\frac{MW}{cm^2}\right] = E[Mev] \cdot 10^{-4} |J| \left[\frac{A}{m^2}\right] = 0.5109989 \cdot 10^{-4} \gamma |J| \left[\frac{A}{m^2}\right]$$

[4] The concept of saturation intensity for FEL devices has been systematically used after the publication of the paper S. Cabrini, G. Dattoli and L. Giannessi, Phys. Rev. A 44, 8433 (1991).

2 - FEL GAIN AND SATURATION INTENSITY

We denote G_M as the maximum gain and $G(g_0,\nu)$ as the gain function containing either the dependence on the small signal gain coefficient and the detuning.

2.1 Homogeneous broadening case[5]

$g_0 \le 10$

$$G_M = G(g_0) \cong 0.85 g_0 + 0.192 g_0^2 + 4.23\cdot 10^{-3} g_0^3 \qquad 2.1)$$

$$G(g_0,\nu) \cong \sum_{s=1}^{3} g_0^s g_s(\nu)$$

$$g_1(\nu) = \frac{2\pi}{\nu^3}\left[2\,(1-cos(\nu)) - \nu\, sin(\nu)\right]$$

$$g_2(\nu) = \frac{\pi^2}{3\nu^6}\left[84(1-cos(\nu)) - 60\nu\, sin(\nu) + 3\nu^2 + 15\nu^2\, cos(\nu) + \nu^3\, sin(\nu)\right] \qquad 2.2)$$

$$g_3(\nu) = \frac{\pi^3}{60\nu^9}\left[11520(1-cos(\nu)) - 9000\nu\, sin(\nu) + 360\nu^2 + 2880\nu^2\, cos(\nu) + \right.$$
$$\left. + 480\nu^3\, sin(\nu) - 20\nu^4(1+2\,cos(\nu)) - \nu^5\, sin(\nu)\right]$$

for $\nu \to 0$:

$$g_1(\nu) = \frac{\pi}{6}\left(\nu - \frac{\nu^3}{15} + \frac{\nu^5}{560} - \cdots\right)$$

$$g_2(\nu) = \frac{\pi^2}{40}\left(1 - \frac{\nu^2}{28} + \frac{19\nu^4}{45360} - \cdots\right) \qquad 2.3)$$

$$g_3(\nu) = \frac{\pi^3}{1200\times 28}\left(\nu - \frac{7\nu^3}{198} + \frac{19\nu^5}{36036} - \cdots\right)$$

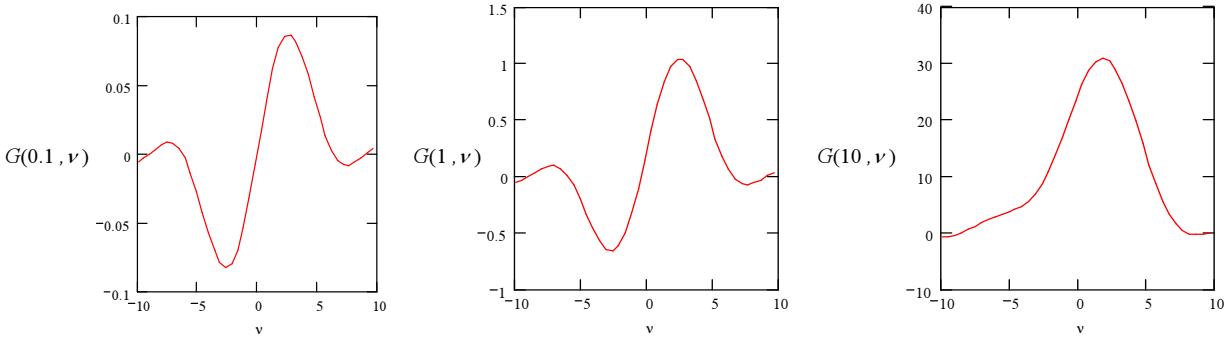

Fig. 2.1 FEL gain for three different values of the small signal gain coefficient a) $g_0 = 0.1$, b) $g_0 = 1$, c) $g_0 = 10$.

[5] We define "low-gain" regime the case in which the higher order corrections in the small signal gain coefficient are negligible. The value of $g_0 = 0.2$ can be safely assumed as an upper limit for the low gain approximation, it produces, indeed, a deviation of about 4% from the exact value.

A particularly useful approximation for integrals computation is

$$g_1(\nu) \cong \frac{\pi}{a_1}\exp\left(-\frac{\nu^2}{b_1}\right)\sin\left(\frac{\nu}{c_1}\right)\cos\left(\frac{\nu}{d_1}\right)\cos\left(\frac{\nu}{e_1}\right)$$
$$g_2(\nu) \cong \frac{\pi^2}{a_2}\exp\left(-\frac{\nu^2}{b_2}\right)\cos\left(\frac{\nu}{c_2}\right)\cos\left(\frac{\nu^2}{d_2}\right)\cos\left(\frac{\nu^2}{e_2}\right) \qquad 2.4)$$
$$g_3(\nu) \cong \frac{\pi^3}{a_3}\exp\left(-\frac{\nu^2}{b_3}\right)\sin\left(\frac{\nu}{c_3}\right)\cos\left(\frac{\nu}{d_3}\right)\cos\left(\frac{\nu}{e_3}\right)$$

with

$a_1 = 3.0$	$b_1 = 209.11$	$c_1 = 2.0$	$d_1 = 5.7212$	$e_1 = 9.8361$
$a_2 = 40.0$	$b_2 = 58.01$	$c_2 = 5.2427$	$d_2 = 78.9575$	$e_2 = 142.589$
$a_3 = 11461$	$b_3 = 128.60$	$c_3 = 2.9317$	$d_3 = 9.0363$	$e_3 = 13.369$

relative error $< 1.7\%$ in the range $|\nu| \le 10$

$g_0 > 10$

$$G_M \cong \frac{1}{9}\left[1+\frac{1}{\sqrt{3}(\pi g_0)^{1/3}}\right]\exp\left[\sqrt{3}(\pi g_0)^{1/3}\right]$$
$$G(g_0,\nu) \cong \frac{1}{9}\left[1+(6-\sqrt{3}\nu)\frac{\nu}{9(\pi g_0)^{1/3}}\right]\exp\left[\sqrt{3}(\pi g_0)^{1/3}\right] \qquad 2.5)$$

The value of the detuning yielding the maximum gain ν_M is a function of g_0 and decreases with increasing g_0, for $g_0 \le 100$ it can be reproduced by the relation

$$\nu_M(g_0) \cong 2.6 - 1.1\left[1-\exp(-0.14 g_0)\right] \qquad 2.6)$$

The saturation intensity decreases with increasing g_0 and a practical formula for $g_0 \le 20$ is

$$I_S(g_0) = \frac{1.078 \cdot I_S}{P(g_0)}; \qquad P(g_0) = 1 + 0.19\, g_0 - 8.7\cdot 10^{-3} g_0^2 + 2.7\cdot 10^{-4} g_0^3 \qquad 2.7)$$

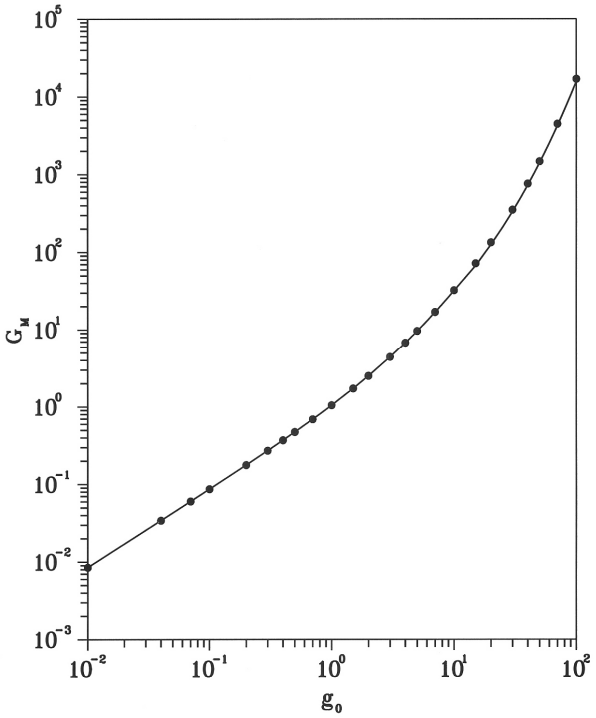

Fig. 2.2 Maximum gain versus g_0 with no broadening effects; dot: 1-D simulation, continuous line: formulae 2.1) and 2.5). Relative error <1% for $g_0 \leq 10$, <7% for $g_0 \leq 100$

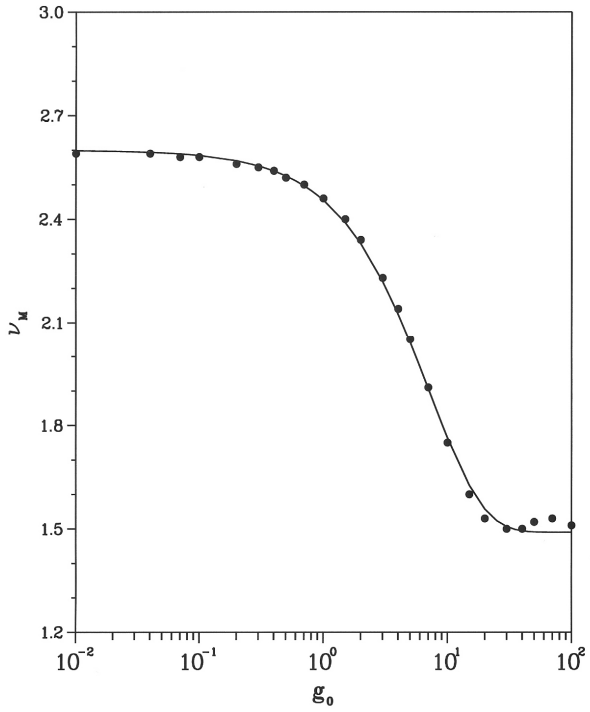

Fig. 2.3 Detuning parameter ν yielding the maximum gain versus g_0 with no broadening effects; dot: 1-D simulation, continuous line: formula 2.6). Relative error <3%.

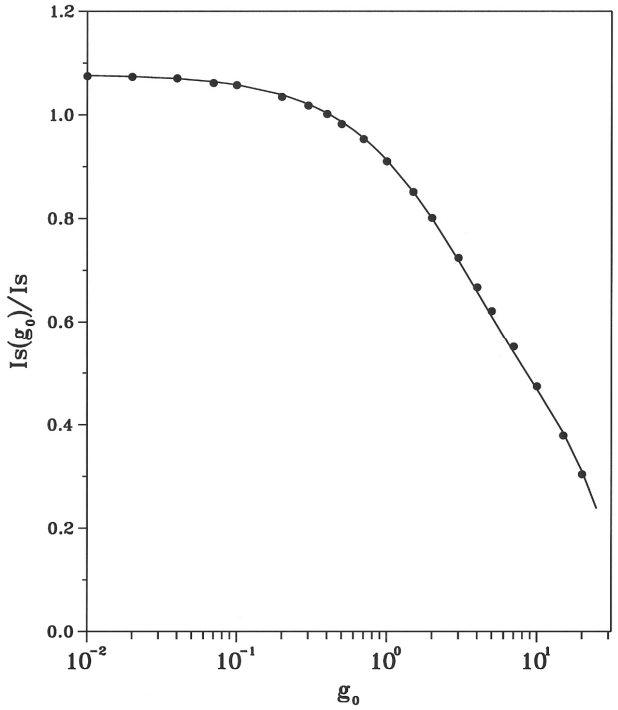

Fig. 2.4 Saturation intensity versus g_0 with no broadening effects; dot: 1-D simulation, continuous line: formula 2.7). Relative error <2% for $g_0 \leq 20$

2.2 Energy spread corrections

For $g_0 \le 10$ and $\mu_\varepsilon \le 1$.[6]

$$\frac{G_M(g_0,\mu_\varepsilon)}{G_M} = \frac{exp\left[-0.132\,P(g_0)\mu_\varepsilon^2\right]}{1+1.6Q(g_0)\mu_\varepsilon^2} \qquad with \tag{2.8}$$

$$P(g_0) = 1 - 3.57\cdot 10^{-3} g_0 + 6.83\cdot 10^{-2} g_0^2 - 4.79\cdot 10^{-3} g_0^3$$
$$Q(g_0) = 1 + 0.142 g_0 - 0.011 g_0^2 + 1.8\cdot 10^{-4} g_0^3$$

$$\frac{\nu_M(g_0,\mu_\varepsilon)}{\nu_M(g_0)} = 1 + 0.46\,P(g_0)\mu_\varepsilon^2, \qquad P(g_0) = 1 + 0.188 g_0 - 5\cdot 10^{-3} g_0^2 \tag{2.9}$$

$$\frac{I_S(g_0,\mu_\varepsilon)}{I_S(g_0)} = 1 + 2.1P(g_0)\mu_\varepsilon^2 - 0.38\,\mu_\varepsilon^4, \qquad P(g_0) = 1 + 9\cdot 10^{-2} g_0 - 6\cdot 10^{-3} g_0^2 \tag{2.10}$$

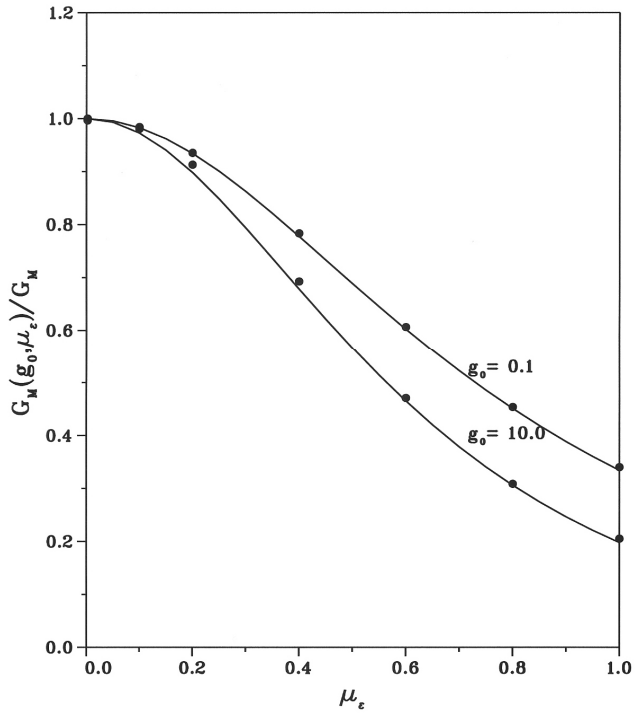

Fig. 2.5 Maximum gain versus energy spread parameter μ_ε for $g_0 = 0.1$ and $g_0 = 10$; dot: 1-D simulation, continuous line: formula 2.8). Relative error <3.5%.

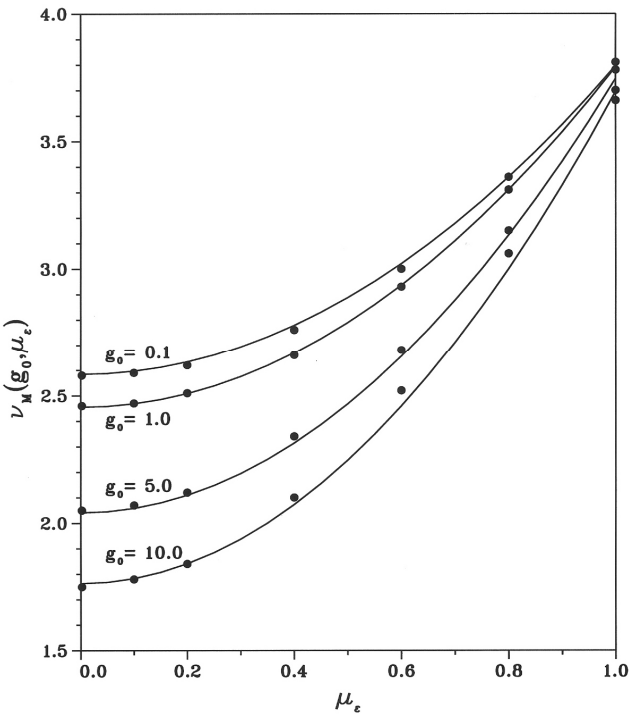

Fig. 2.6 Detuning parameter ν yielding the maximum gain versus μ_ε for different values of g_0; dot: 1-D simulation, continuous line: formula 2.9). Relative error <2.5%.

[6] In the case of low gain regime the inhomogeneous broadening effect is reproduced by $G_M = 0.85\frac{g_0}{1+1.7\mu_\varepsilon^2}$, the fit with the coefficient 1.6, appearing in eq. (2.8) yields a smaller error when high gain corrections are included.

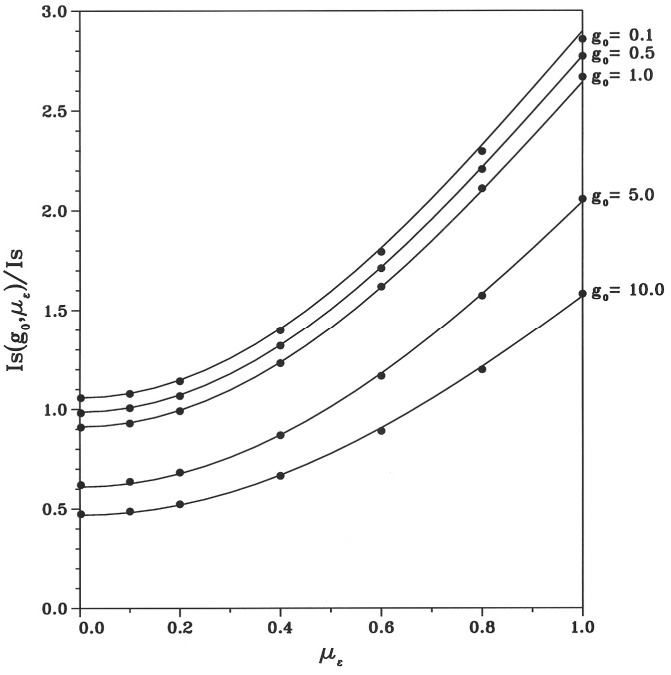

Fig. 2.7 Saturation intensity versus μ_ε for different values of g_0; dot: 1-D simulation, continuous line: formula 2.10). Relative error <2%.

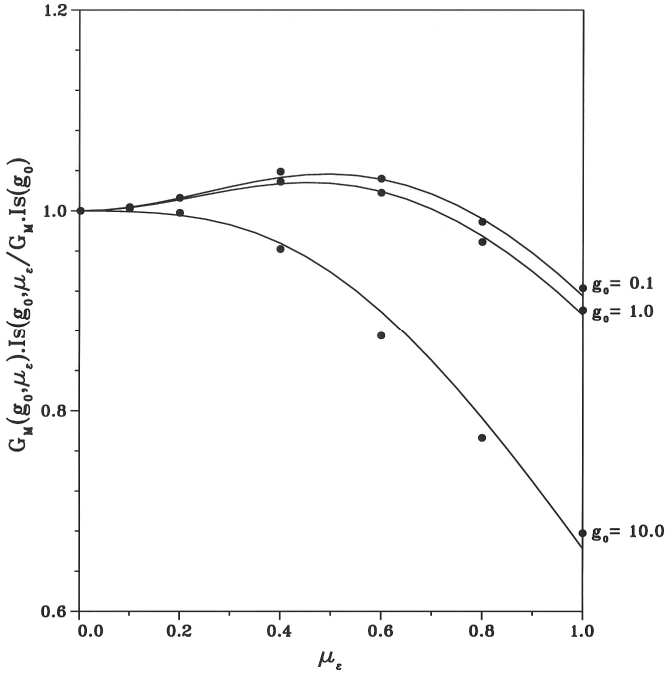

Fig. 2.8 Maximum gain and saturation intensity product versus μ_ε for different values of g_0. Dot: 1-D simulation, continuous line: formulae 2.8), 2.10). Relative error <3%.

The gain and the saturation intensity have opposite behaviour with increasing inhomogeneous broadening parameter. In fact, in low gain regime, the product $G_M I_S$ is nearly a constant satisfying the condition (see sect. 1.13)

$$\frac{G_M I_S}{0.85 P_E} \leq \frac{1}{2N} \qquad 2.11)$$

This quantity represents the intrinsic FEL efficiency which remains, within large limits, not affected by inhomogeneous broadening effects.
As can be seen in Fig. 2.8, the product remain a constant for values of μ_ε up to 1 if we limit ourselves to the moderate gain regime ($g_0 \leq 1$).

2.3 Emittance corrections (matched and round e-beam case)

For $g_0 \leq 0.2$, $\mu_x, \mu_y \leq 1$

In low gain regime the use of integral representation for the field amplitude allows to derive the following expression for the gain including emittance corrections:

$$G(g_0,\nu,\mu_x,\mu_y)=G_M\cdot g_1(\nu,\mu_x,\mu_y)$$

$$g_1(\nu,\mu_x,\mu_y)=\frac{-2\pi}{0.84849}\int_0^1\frac{t(1-t)}{F(t)}G(t)dt \qquad 2.12)$$

$$F(t)=\left[1+(\pi\mu_x t)^2\right]\cdot\left[1+(\pi\mu_y t)^2\right]$$

$$G(t)=\pi(\mu_x+\mu_y)\,t\,cos(\nu t)-(1-\pi^2\mu_x\mu_y t^2)\,sin(\nu t)$$

From above equations the maximum gain as function of μ_x,μ_y can be derived.
For $\mu_x=\mu_y=\mu$ we get the following fit formulas

$$G_M(g_0,\mu)=G_M\,g_1(\mu)$$

$$g_1(\mu)=\frac{1}{(1+\mu^2)^2}P(\mu),\qquad P(\mu)=1-0.0108\mu-1.531\mu^2+2.39\mu^3-0.934\mu^4 \qquad 2.13)$$

$$\nu_M(\mu)=2.6[1+3.757(1-exp(-0.683\mu))] \qquad 2.14)$$

$$\frac{I_S(g_0,\mu)}{I_S(g_0)}=\frac{(1+\mu^2)^2}{Q(\mu)},\qquad Q(\mu)=1-0.28\mu-0.54\mu^2+1.90\mu^3-0.51\mu^4 \qquad 2.15)$$

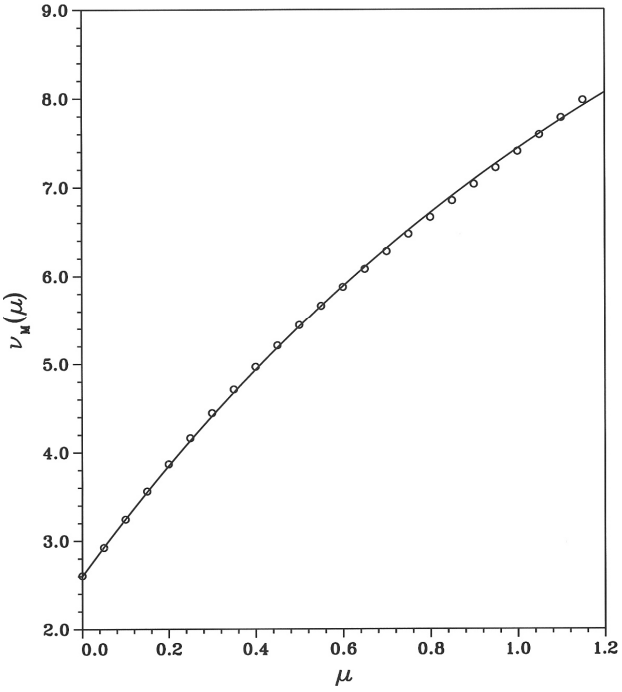

Fig. 2.9 Detuning versus emit parameter yielding the maximum gain. Dot: from eq. 2.12), continuous line: formula 2.14). Relative error <1%.

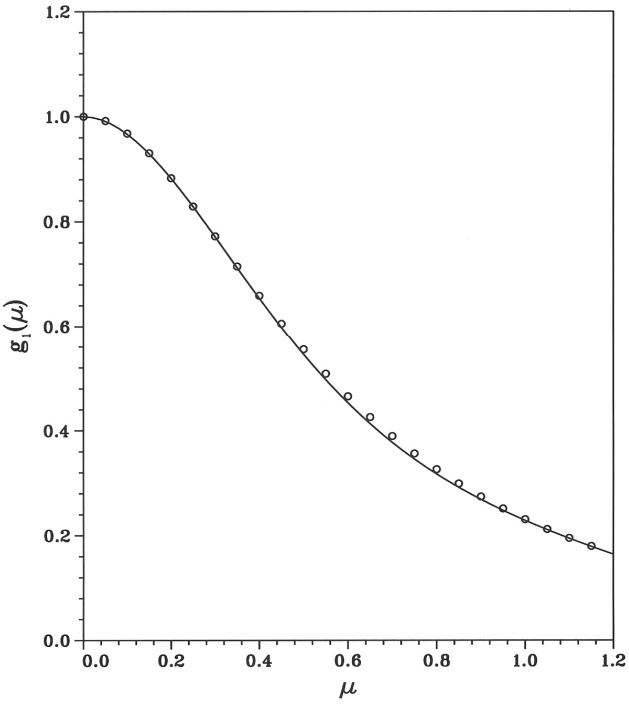

Fig. 2.10 Maximum gain versus emit parameter. Dot: from eq. 2.12), continuous line: formula 2.13). Relative error <3%.

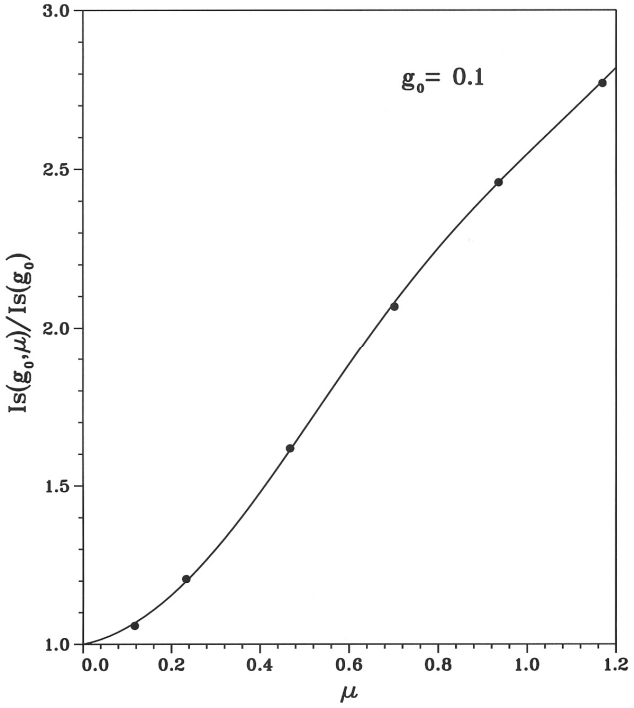

Fig. 2.11 Saturation intensity versus μ for g_0=0.1. Dot: 1-D simulation, line formula 2.15). Relative error <1%.

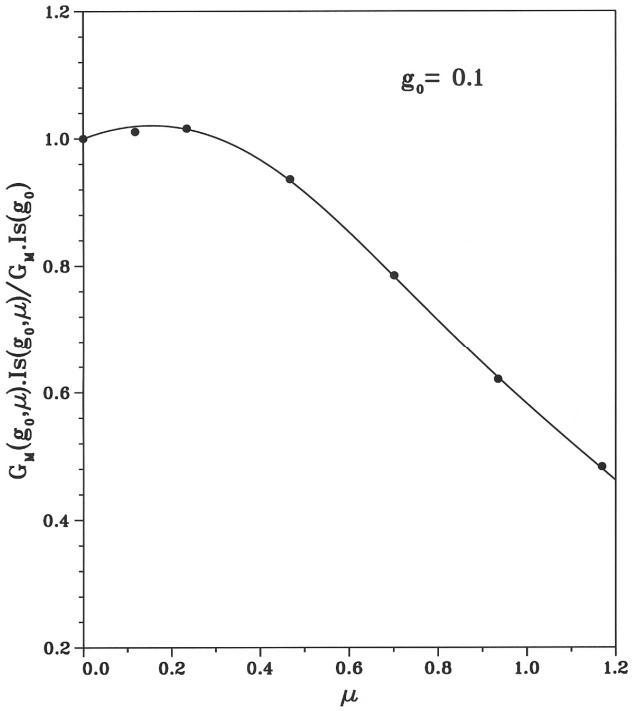

Fig. 2.12 Maximum gain and saturation intensity product versus μ for g_0=0.1. Dot: 1-D simulation, continuous line: formulae 2.13), 2.15). Relative error <1%.

For the product $G_M I_S$ the same considerations holds as for the inhomogeneous broadening effects. As can be seen in Fig. 2.12 the FEL efficiency remains nearly independent for values of the μ parameters below 0.4.

2.4 Combined effects of energy spread and emittance

For $g_0 \le 0.2$, $\mu_x, \mu_y \le 1$, $\mu_\varepsilon \le 1$

$$G_M(g_0,\mu_\varepsilon,\mu) = \frac{G_M\, g_1(\mu)}{1+1.6\, g_1(\mu)\mu_\varepsilon^2} exp\left(-0.132\mu_\varepsilon^2\right) \qquad 2.16)$$

$$\frac{\nu_M(g_0,\mu_\varepsilon,\mu)}{\nu_M(g_0)} = \frac{\nu_M(g_0,\mu)}{\nu_M(g_0)} + 0.46\left(1+0.188 g_0\right)\mu_\varepsilon^2 + 0.473\mu^{1.436}\cdot\mu_\varepsilon^{1.409} \qquad 2.17)$$

$$\frac{I_S(g_0,\mu_\varepsilon,\mu)}{I_S} = \frac{I_S(g_0,\mu)}{I_S}\, F(\mu_\varepsilon,\mu), \qquad F(\mu_\varepsilon,\mu) = 1+Q(\mu)\mu_\varepsilon^2 - 0.33\mu_\varepsilon^4 \qquad 2.18)$$

$$Q(\mu) = 1.02 + 0.98 exp\left(-5.46\mu^2\right)$$

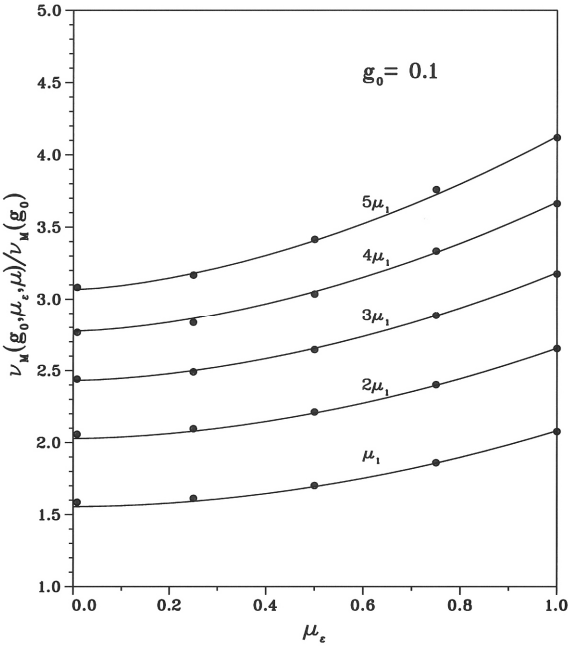

Fig. 2.13 Detuning versus μ_ε yielding the maximum gain for different values of μ: $\mu_1 = 0.234$, g_0=0.1. Dot: 1-D simulation, line: formula 2.17). Relative error <2%.

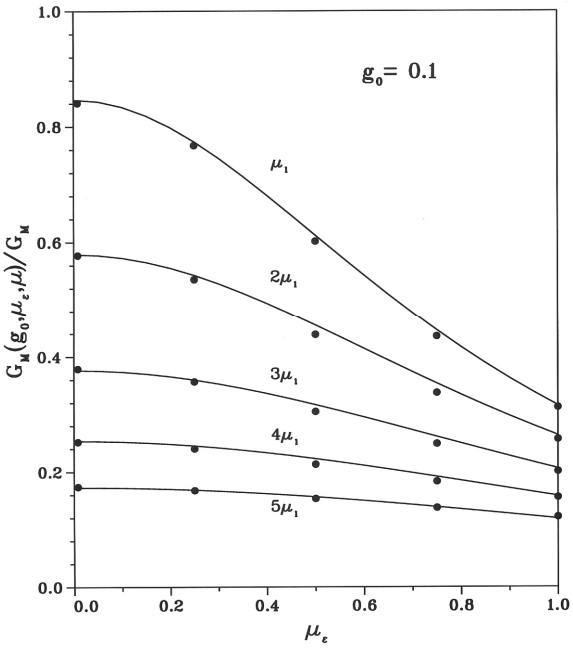

Fig. 2.14 Maximum gain versus μ_ε for different values of μ: $\mu_1 = 0.234$, g_0=0.1. Dot: 1-D simulation, line: formula 2.16). Relative error <5%.

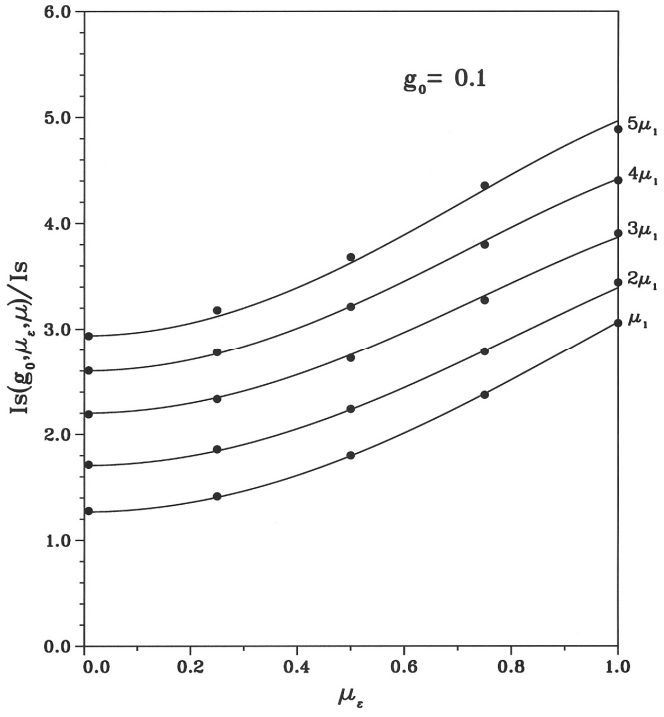

Fig. 2.15 Saturation intensity versus μ_ε for different values of μ: $\mu_1 = 0.234$, g_0=0.1. Dot: 1-D simulation, line formula 2.18). Relative error <2%.

2.5 Gain saturation formula

$$G(\eta, X) = \frac{G_M(\eta)}{F(X)}, \qquad X = \frac{I}{I_S(\eta)} \tag{2.19}$$

$$F(X) = 1 + \alpha\, X + \beta\, X^2, \qquad \alpha + \beta = 1, \qquad \alpha = 2\left(\sqrt{2} - 1\right), \quad \beta = 3 - 2\sqrt{2}$$

Here η indicates a set of parameters like $g_0, \mu_\varepsilon, \mu$, the function $F(X)$ being independent on inhomogeneous broadening effects. Figs. 2.16a, b give an example for different g_0 and μ_ε values.

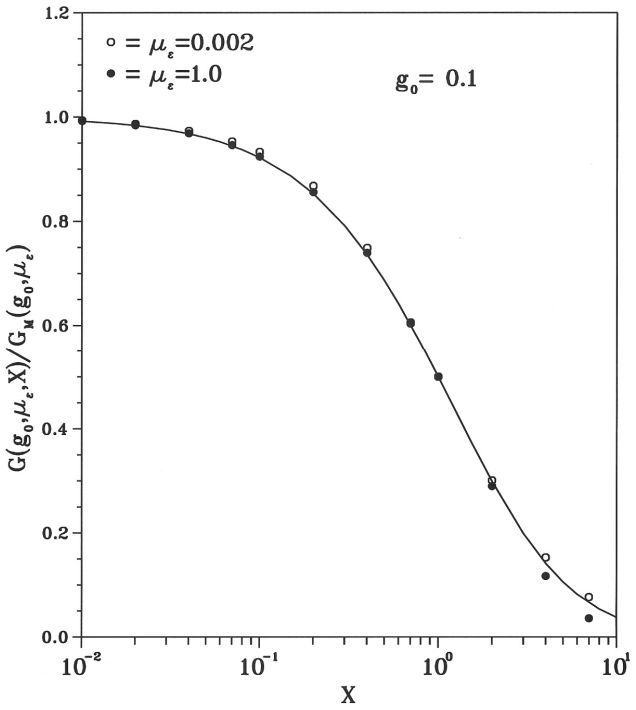

Fig. 2.16a Gain versus X for $\mu_\varepsilon \approx 0$ and $\mu_\varepsilon = 1$, g_0=0.1. Dots: 1-D simulation, line: formula 2.19). Relative error <3% for $X \le 2$.

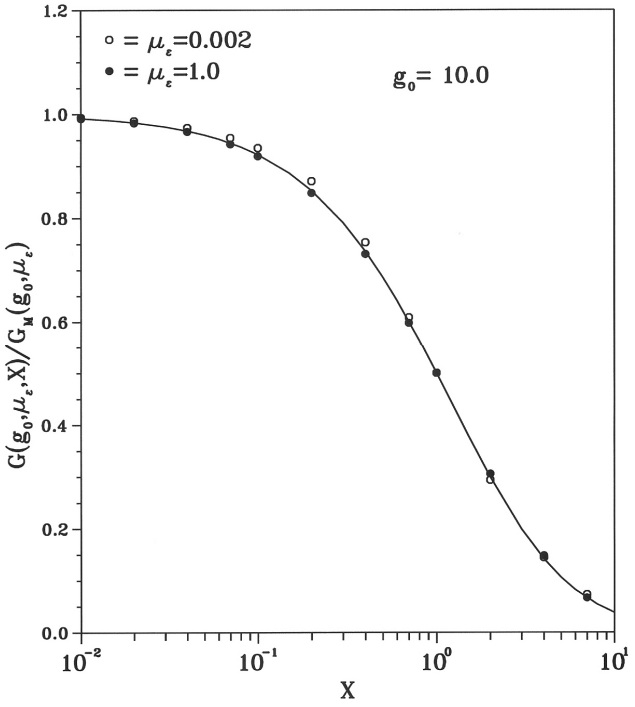

Fig. 2.16b Gain versus X for $\mu_\varepsilon \approx 0$ and $\mu_\varepsilon = 1$, g_0=10. Dots: 1-D simulation, line: formula 2.19). Relative error <3 % for $X \le 2$.

3 - HIGH GAIN AMPLIFIER AND NON-LINEAR HARMONIC GENERATION

3.1 Colson equations including harmonic generation

$$\frac{d^2}{d\tau^2}\zeta = \sum_{n=0}^{\infty} |a_n| cos(\psi_n), \quad \psi_n = n\zeta + \phi_n$$

$$\frac{d}{d\tau} a_n = -j_n \left\langle e^{-in\zeta} \right\rangle \qquad 3.1)$$

$$j_n = 2\pi\, g_{0,n}$$

where

n = *harmonic number (odd ones for linear undulator, n=1 only for helical undulator)*

a_n = *dimensionless amplitude*

ϕ_n = *field amplitude phase*

j_n = *dimensionless current*

$a_1,\ \phi_1, j_1$ corresponds to $a,\ \phi, j$ of previous sections.

$$g_{0,n} = g_0 \left(\frac{f_{b,n}}{f_{b,1}} \right)^2 \qquad \textit{small signal gain coefficient}$$

$$f_{b,n}(\xi) = (-1)^{\frac{n-1}{2}} \left[J_{\frac{n-1}{2}}(n\xi) - J_{\frac{n+1}{2}}(n\xi) \right] \qquad \textit{Bessel function factor} \qquad 3.2)$$

$$\rho_n = \frac{1}{4\pi} \left[\frac{\pi\, g_{0,n}}{N^3} \right]^{\frac{1}{3}} = \rho_1 \left[\frac{f_{b,n}}{f_{b,1}} \right]^{\frac{2}{3}} \qquad \textit{Pierce parameter} \qquad 3.3)$$

$$L_{g,n} = \frac{\lambda_u}{4\pi\sqrt{3}\rho_n} \qquad \textit{gain length} \qquad 3.4)$$

3.2 Fundamental harmonic

$$P_{F,1} = \sqrt{2}\rho_1 P_E \qquad \textit{saturated power (maximum achievable power)} \qquad 3.5)$$

$$Z_{F,1} = 1.066\, L_{g,1}\, ln\left(\frac{9P_{F,1}}{P_0} \right) \qquad \textit{saturation length} \qquad 3.6)$$

P_0 *input seed power*

In the case of high gain amplifier devices having

$$\rho_1 \cong \frac{1}{N}, \qquad g_{0,1} \cong \frac{(4\pi)^3}{\pi} \qquad 3.7)$$

a quick evaluation of the maximum gain and of the final intensity yields

$$G \cong \frac{1}{9} e^{4\pi\sqrt{3}} \cong 3.15 \cdot 10^{8}$$
$$I_F \cong \frac{2\sqrt{2}}{\pi} (4\pi)^3 I_S \cong 1.79 \cdot 10^{3} I_S \qquad 3.8)$$

Logistic function power growth (fast growing root only) without lethargy contribution (see Appendix C)

$$P_1(z) = \frac{P_0}{9} \frac{exp\left(a\frac{z}{Z_{F,1}}\right) exp\left(\frac{z}{L_{g,1}}\right)}{1 + \frac{P_0}{9P_{F,1}}\left[exp\left(\frac{z}{L_{g,1}}\right) - 1\right]}, \quad a \cong 0.223, \quad z \ \textit{longitudinal coordinate} \qquad 3.9)$$

Power growth including lethargy

$$P_1(z) = P_0 \frac{A(z) exp\left(a\frac{z}{Z_{F,1}}\right)}{1 + \frac{P_0}{P_{F,1}}[A(z) - 1]} \qquad 3.10)$$
$$A(z) = \frac{1}{9}\left[3 + 2cosh\left(\frac{z}{L_{g,1}}\right) + 4cos\left(\frac{\sqrt{3}}{2}\frac{z}{L_{g,1}}\right) cosh\left(\frac{z}{2L_{g,1}}\right)\right]$$

FEL induced relative energy spread

$$\sigma_i(z) \cong 3C\sqrt{\frac{A(z)}{1 + 9B[A(z) - 1]}}$$

$$C = \frac{1}{2}\sqrt{\frac{\rho_1 P_0}{P_E}}, \qquad B \cong \frac{1.24}{9}\frac{P_0}{P_{F,1}} \qquad 3.11)$$
$$\sigma_{i,F} \cong \frac{C}{\sqrt{B}} \cong 1.6\rho_1$$

The total energy spread is

$$\sigma_\varepsilon(z) = \left[\sigma_{\varepsilon,0}^2 + \sigma_i^2(z)\right]^{1/2}, \qquad \sigma_{\varepsilon,0} = \sigma_\varepsilon(0) \qquad 3.12)$$

The undulator length necessary to reach an induced energy spread $\sigma_i = \frac{\rho_1}{2}$ is

$$Z_B \cong 0.94 Z_{F,1} - 2.44 L_{g,1} \qquad 3.13)$$

3.3 Inhomogeneous broadening effects

Inhomogeneous broadening parameters (see secs. 1.8 and 1.9)

$$\tilde{\mu}_\varepsilon = \frac{2\sigma_\varepsilon}{\rho_1}, \quad \tilde{\mu}_\eta = \frac{E_\eta}{\gamma_\eta}\gamma_N^2, \quad \tilde{\mu}_{\eta'} = \frac{E_\eta}{\beta_\eta}, \quad \alpha_\eta = 0, \quad \eta = x, y$$

$$\gamma_N = \frac{1}{\beta_N}, \quad \beta_N \qquad \textit{undulator eigen} - \textit{beta} \tag{3.14}$$

$$E_\eta = \varepsilon_\eta \frac{\gamma^2}{\rho_1}\left(1 + K^{*2}\right)^{-1}$$

Saturated power and saturation length, eqs. 3.5) and 3.6), are replaced by

$$P_{F,1}(\chi) = \sqrt{2}\ \Phi(\chi)\rho_1 P_E \tag{3.15}$$

$$Z_{F,1}(\chi) = 1.066\ L_{g,1}(\chi) ln\left(\frac{9P_{F,1}(\chi)}{P_0}\right) \tag{3.16}$$

$$L_{g,1}(\chi) = \chi\ L_{g,1}$$

$$\Phi(\chi) = \exp\left[-\chi(\chi - 1)\right] + \sqrt{2}\ \frac{\chi - 1}{\chi^3} \tag{3.17}$$

$$\chi = F_3^{-1}, \qquad F_3 = \frac{F_1}{F_2}\exp\left(c\tilde{\mu}_\varepsilon^2\right)$$

$$F_1 = \frac{1 + a\left(\tilde{\mu}_x^2 + \tilde{\mu}_{x'}^2 + \tilde{\mu}_y^2 + \tilde{\mu}_{y'}^2\right) + b\left(\tilde{\mu}_x + \tilde{\mu}_{x'} + \tilde{\mu}_y + \tilde{\mu}_{y'}\right)}{\sqrt{\left(1 + \tilde{\mu}_x^2\right)\left(1 + \tilde{\mu}_{x'}^2\right)\left(1 + \tilde{\mu}_y^2\right)\left(1 + \tilde{\mu}_{y'}^2\right)}}, \qquad F_2 = 1 + d\ F_1\ \tilde{\mu}_\varepsilon^2$$

$$a = 0.159, \quad b = -0.066, \quad c = -0.034, \quad d = 0.185\ \frac{\sqrt{3}}{2} = 0.1602$$

If $\tilde{\mu}_\eta$, $\tilde{\mu}_{\eta'}$ are negligible $F_1 = 1$ and χ reduces to $\chi = \left(1 + d\ \tilde{\mu}_\varepsilon^2\right) exp\left(-c\ \tilde{\mu}_\varepsilon^2\right)$.

The high gain power growth is reproduced by logistic type equations, upon replacing

$$L_{g,1}(\chi) \to L_{g,1}, \qquad P_{F,1}(\chi) \to P_{F,1} \tag{3.18}$$

3.4 Diffraction correction

$$\mu_\eta^D = \frac{\lambda_0 \lambda_u}{(4\pi)^2 \beta_\eta \varepsilon_\eta \rho_1} \qquad \textit{diffraction correction parameter}$$

$$\rho_1^D = F\left(\mu_x^D, \mu_y^D\right)\rho_1 \tag{3.19}$$

$$F\left(\mu_x^D, \mu_y^D\right) = \left[\left(1 + \mu_x^D\right)\left(1 + \mu_y^D\right)\right]^{-1/6}$$

Previously defined quantities maintain the same expressions provided that $\rho_1^D \to \rho_1$, obtaining, e.g., a function χ^D in place of χ.

The saturated power results

$$P_{F,1} = \sqrt{2}\,\Phi\left(\chi^D\right)\rho_1^D\,P_E \qquad 3.20)$$

This equation yields a slightly larger value than the one predicted by the Xie formula[7]. A closer agreement is obtained by a reducing factor $\frac{\rho_1^D}{\rho_1}$

$$P_{F,1} = \left(\frac{\rho_1^D}{\rho_1}\right)^2 \sqrt{2}\,\Phi\left(\chi^D\right)\rho_1 P_E \qquad 3.21)$$

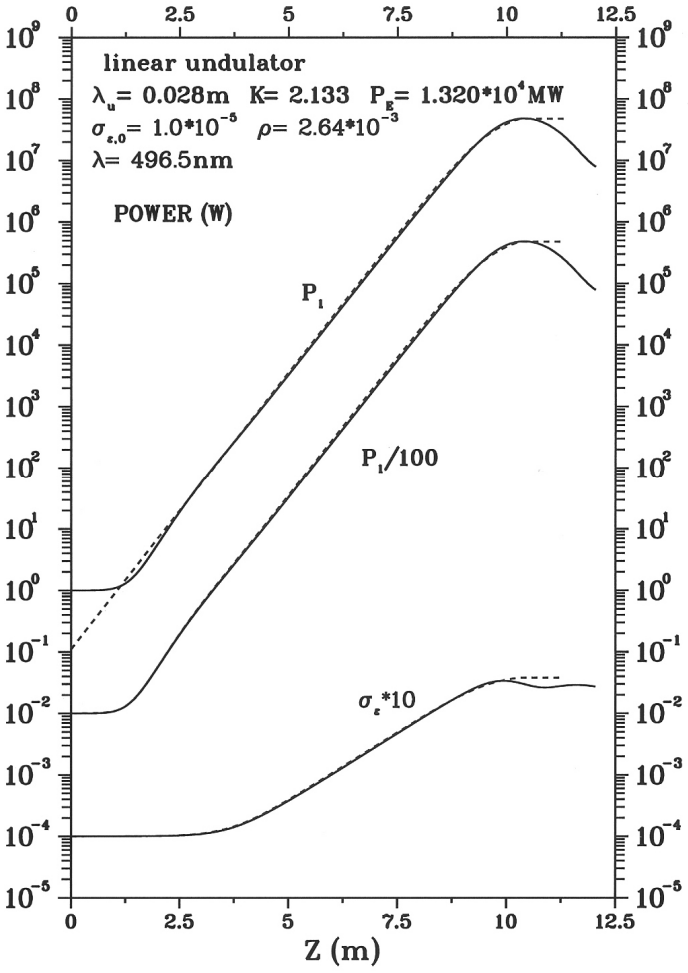

Fig. 3.1 Main harmonic power and energy spread evolution.
Upper curves - continuous line: 1-D simulation, dashed line: eq. 3.9).
Middle curves – continuous line: 1-D simulation, dashed line: eq. 3.10).
Lower curves - continuous line: 1-D simulation, dashed line: eqs. 3.11), 3.12).

[7] M. Xie, *IEEE Proc. for particle accelerator Conference 95* (IEEE, New York, 1996), p. 183, Paper N 95CH3584.

3.5 Bunching coefficients

$$b_n = \left\langle e^{in\zeta} \right\rangle \qquad n \text{ positive integer} \qquad 3.22)$$

The bunching generated by main harmonic in the exponential power growth part is characterized by

$$|b_n(z)|^2 = \alpha_n \left(\frac{P_1(z)}{\rho_1 P_E} \right)^n \qquad 3.23)$$

For $n \le 5$:

$$\alpha_1 = 1, \quad \alpha_2 = \frac{20}{9}, \quad \alpha_3 = 6, \quad \alpha_4 = \frac{56}{3}, \quad \alpha_5 = 60$$

As an example in Figs. 3.2, 3.3 the first five bunching coefficients evolution is shown for linear (without generation of subharmonics) and helical undulator configurations.

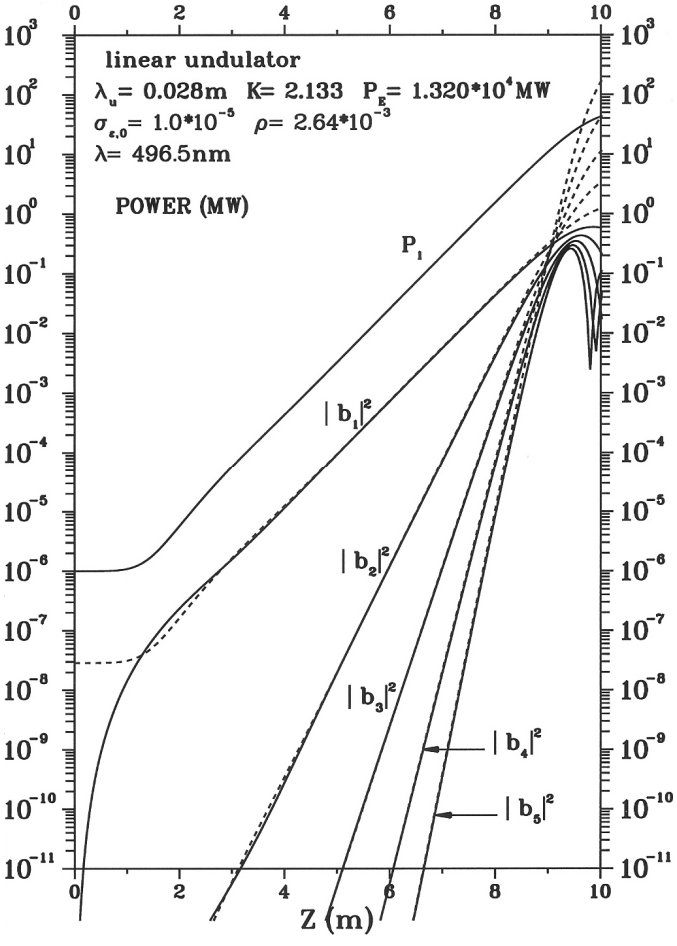

Fig. 3.2 Main harmonic power and bunching coefficients for linear undulator. Continuous line:1-D simulation, dashed line: eqs. 3.23)

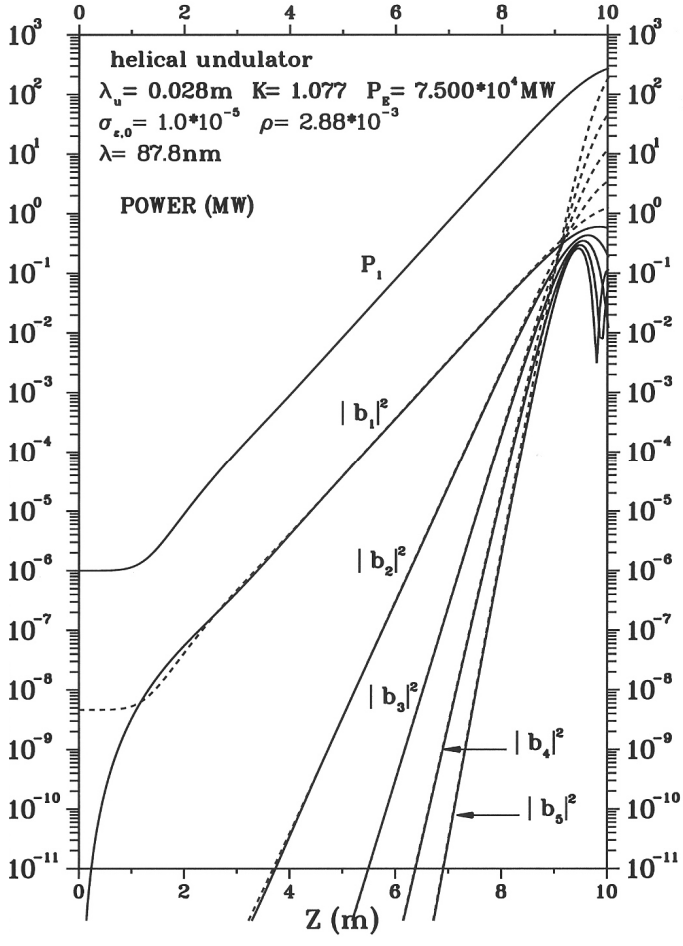

Fig. 3.2 Main harmonic power and bunching coefficients for helical undulator. Continuous line:1-D simulation, dashed line: eqs. 3.23)

It can be seen that the behaviour of $|b_1|^2$ in the lethargic region is not reproduced by eq. 3.23); a perfect agreement with simulation results in all region is given by the following formula (Fig. 3.4)

$$|b_1(z)|^2 = P_b \frac{B_l(z)}{\rho_1 P_E}, \qquad B_l(z) = \frac{B(z)}{1+\frac{P_b}{P_{F,1}} B(z)}, \qquad P_b = \frac{P_0}{9}$$

$$B(z) = 2\left[cosh\left(\frac{z}{L_{g,1}}\right) - exp\left(-\frac{z}{2L_{g,1}}\right) cos\left(\frac{\pi}{3}+\frac{\sqrt{3}z}{2L_{g,1}}\right) - exp\left(\frac{z}{2L_{g,1}}\right) cos\left(\frac{\pi}{3}-\frac{\sqrt{3}z}{2L_{g,1}}\right)\right] \qquad 3.24)$$

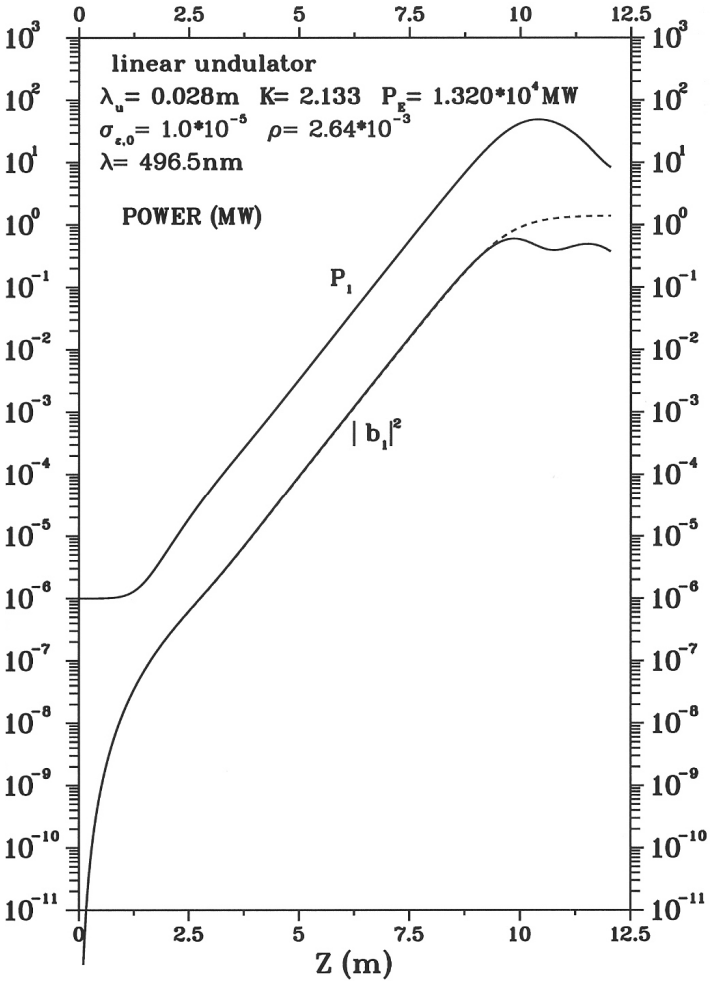

Fig. 3.4 Main harmonic power and $|b_1|^2$ evolution. Continuous line: 1-D simulation, dashed line: eq.3.24), overlapping the continuous one except in the saturation region

3.6 Higher harmonics generation (linear undulator)

Higher harmonic power evolution in a high gain FEL amplifier is shown in Fig. 3.5 for $n = 3, 5$.

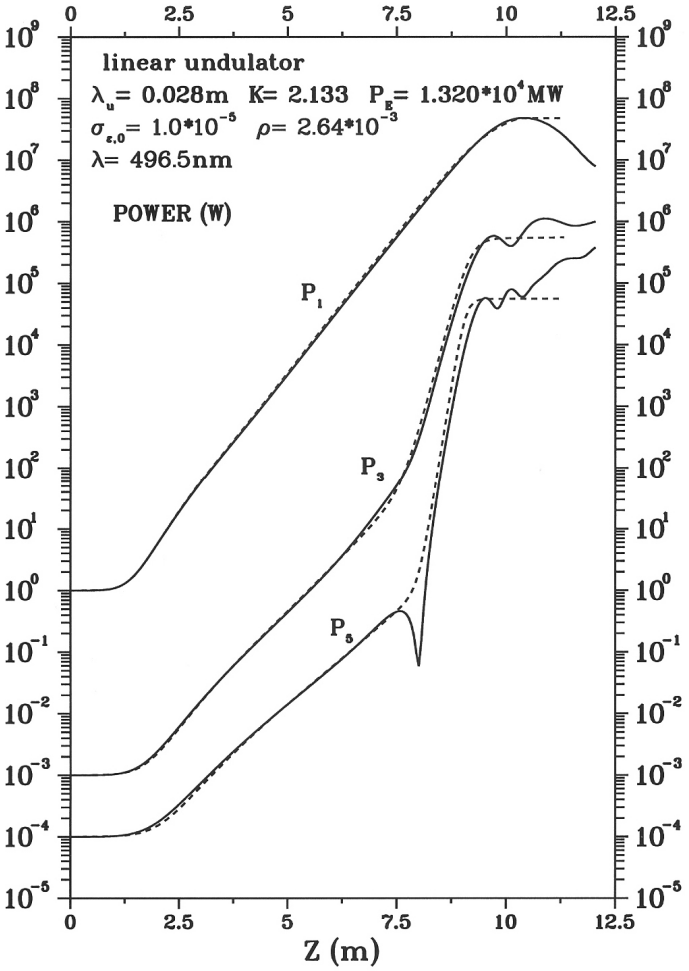

Fig. 3.5 Power growth of the first three harmonics in a high gain FEL amplifier. Continuous line: 1-D simulation, dashed lines: theoretical formulas 3.10) for $P_1(z)$ and 3.25), 3.27), 3.29) for $P_3(z)$ and $P_5(z)$.

The first part of the evolution, indicated as $\Lambda_n(z)$, is the linear contribution, the second one, denoted by $\Pi_n(z)$, specifies the non linear contribution induced by the bunching due to the fundamental.

$$P_n(z) = \Lambda_n(z) + \Pi_n(z), \qquad n = 3, 5, 7 \ldots \tag{3.25}$$

$$\Lambda_n(z) = \frac{P_{0,n}}{9} exp\left(\frac{z}{L^*_{g,n}}\right) \qquad \textit{without lethargy contribution} \tag{3.26}$$

$$\Lambda_n(z) = P_{0,n}\, A_n(z) \qquad \textit{with lethargy contribution} \tag{3.27}$$

where

$$L^*_{g,n} = \frac{\lambda_u}{4\pi\sqrt{3}\rho^*_n} = n^{-1/3} L_{g,n}\,, \qquad \rho^*_n = n^{1/3}\rho_n \tag{3.28}$$

$P_{0,n}$ *input seed power*

and $A_n(z)$ is given by $A(z)$ of eq. 3.10) with $L_{g,1}$ substituted by $L^*_{g,n}$.

$$\Pi_n(z) = \Pi_{0,n} \frac{exp\left(\frac{n z}{L_{g,1}}\right)}{1 + \frac{\Pi_{0,n}}{\Pi_{F,n}}\left[exp\left(\frac{n z}{L_{g,1}}\right) - 1\right]} \qquad 3.29)$$

with

$$\Pi_{0,n} = c_n \left(\frac{P_0}{9\,\rho_1 P_E}\right)^n \Pi_{F,n}, \qquad c_3 = 8, \quad c_5 = 116 \qquad 3.30)$$

$$\Pi_{F,n} = \sqrt{n}\left(\frac{\rho_n}{n\,\rho_1}\right)^3 P_{F,1} = \frac{1}{\sqrt{n}}\left(\frac{f_{b,n}}{n\,f_{b,1}}\right)^2 P_{F,1} \qquad 3.31)$$

where $\Pi_{F,n}$ is an estimate of the maximum of the harmonic power.
The bunching coefficient evolution, in presence of subharmonic generation, is given by (Fig. 3.6)

$$|b_n(z)|^2 = n\frac{P_{b,n}}{\rho_n^* P_E} B_n(z) + \alpha_n \left(\frac{P_1(z)}{\rho_1 P_E}\right)^n \qquad n = 3, 5$$
$$P_{b,n} = \frac{P_{0,n}}{9} \qquad 3.32)$$

where in the first term $B_n(z)$ is the function 3.24) with $L_{g,n}^*$ instead of $L_{g,1}$ and the second term is from eq. 3.23).

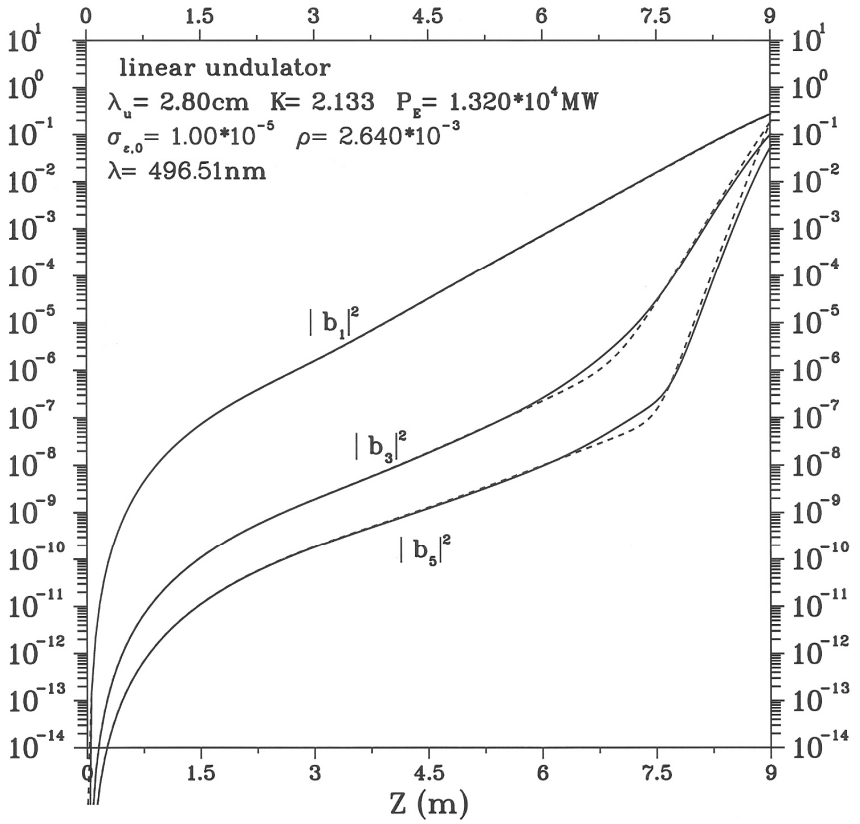

Fig. 3.6 Evolution of bunching coefficients. Continuous line: 1-D simulation, dashed lines: theoretical formula 3.24) for $|b_1|^2$ and 3.32) for $|b_n|^2$, $n = 3, 5$.

3.7 Segmented undulators

FEL operating with segmented (linear or helical) undulators in the SASE mode employ two (or more) undulators sections, tuned at the same wavelength or arranged in such a sequence that each undulator is tuned at a sub-harmonic of the preceding one. We consider negligible seeding in these subsequent sections so that the field growth is initially dominated by the electron bunching.
We first deal with sections with same undulator parameters (Fig. 3.7). The power growth evolution of the main harmonic, in sections after the first one, is well reproduced by

$$P_1(z) = P_b \frac{F(z)}{1+\frac{P_b}{P_{F,1}}F(z)}, \qquad P_b = \left|b_{1,0}\right|^2 \frac{\rho_1 P_E}{2}$$
$$F(z) = 2\left[\cosh\left(\frac{z}{L_{g,1}}\right) - \cos\left(\frac{z}{2L_{g,1}}\right)\cosh\left(\frac{z}{2L_{g,1}}\right)\right] \qquad 3.33)$$

where z refers to each single section and $\left|b_{1,0}\right|^2$ stands for $\left|b_1(0)\right|^2$.

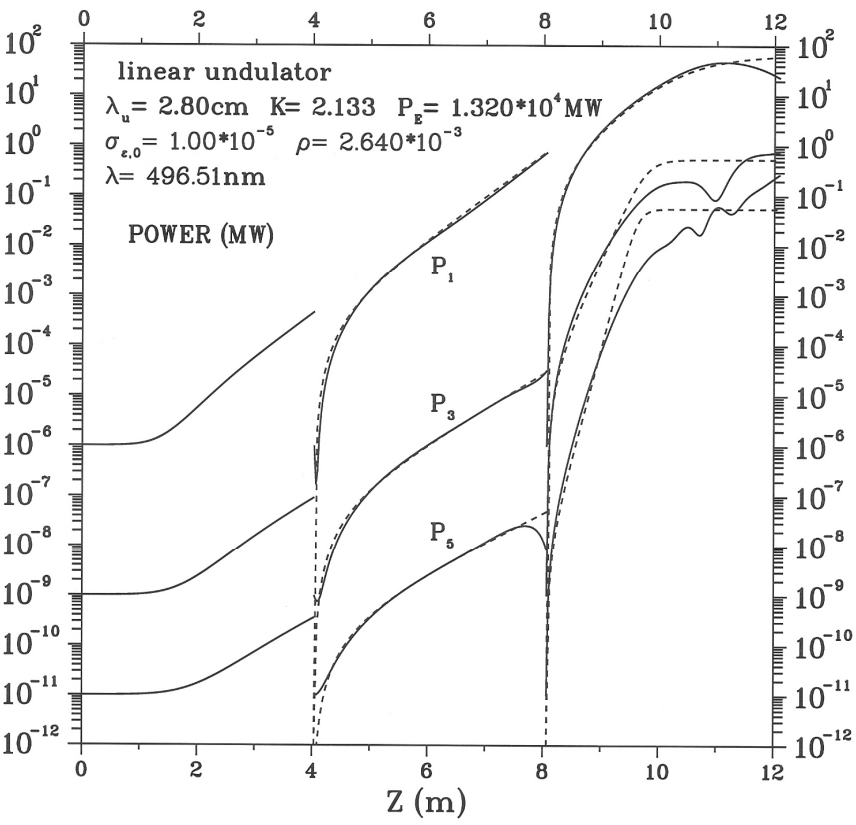

Fig. 3.7 Power growth of the first three harmonics in a three sections undulator with parameters of Fig.3.5. Dispersive zones between sections are not represented. Continuous line: 1-D simulation, dashed lines: theoretical formulae 3.33), 3.34).

The subharmonics growth is reproduced by:

$$P_n(z) = P_{b,n}^L F_n^L(z); \quad P_{b,n}^B \frac{F_n^B(z)}{1+\frac{P_{b,n}^B}{\Pi_{F,n}} F_n^B(z)} \qquad n = 3, 5$$

$$P_{b,3}^L = \frac{9}{2}\left|b_{3,0}\right|^2 \qquad P_{b,5}^L = \frac{5}{2}\left|b_{5,0}\right|^2 \qquad P_{b,n}^B = \left|b_{n,0}\right|^2 \Pi_{F,n} \tag{3.34}$$

in the linear (L) and non-linear (B) regions, $F_n^L(z)$ and $F_n^B(z)$ are given by $F(z)$ of eq. 3.33) with $L_{g,1}$ substituted by $L_{g,n}^*$ and $L_{g,1}/n$ respectively.

From eq. 3.33) it can be deduced that, at the beginning of each section, a length $\Delta z \cong 1.30 L_{g,1}$ is required in order that the main harmonic regains the previous power.

The behaviour of the bunching coefficient $|b_1|$ in sections after the first is described by (Fig. 3.8)

$$|b_1(z)|^2 = |b_{1,0}|^2 \frac{G(z)}{1+|b_{1,0}|^2[G(z)-1]},$$

$$G(z) = cosh\left(\frac{z}{L_{g,1}}\right) + sin\left(\frac{z}{L_{g,1}}\right) cosh\left(\frac{z}{2L_{g,1}}\right) \tag{3.35}$$

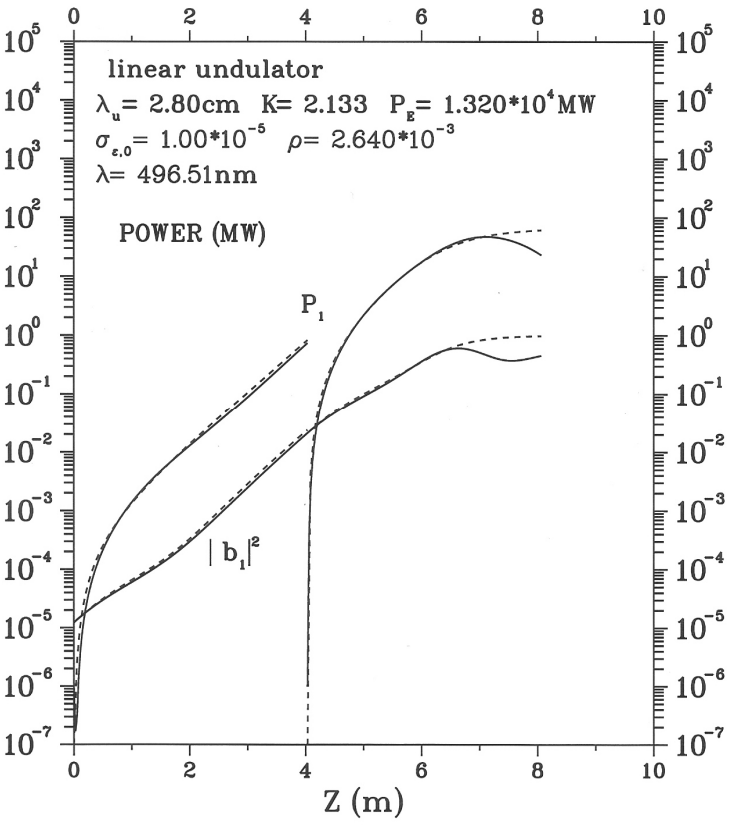

Fig. 3.8 Main harmonic power and $|b_1|^2$ evolution in second and third section of the device of Fig. 3.7). Continuous line: 1-D simulation, dashed line: eq.3.33) and 3.35).

Let us now consider a second section tuned at a subharmonic of the preceding one.
In order to optimize such a device, determined cutting points, Z_c, has to be chosen quite before saturation in the previous section.

In Fig. 3.9 and in Fig. 3.10 we present two simulations with a second undulator section tuned at the second and third harmonic of the first section respectively. The first section parameters in both cases are

$$\lambda_u = 2.8\,cm\,,\quad K = 1.5\,,\quad P_E = 1.32\cdot 10^4\,MW\,,\quad \sigma_{\varepsilon,0} = 10^{-5}\,,\quad \rho_1^I = 2.303\cdot 10^{-3}\,,\quad N = 300$$

The parameters of the second sections are

$\lambda_u = 1.4\,cm\,,\quad K = 1.5\,,\quad \rho_1^{II} = 1.451\cdot 10^{-3}$ if tuned at the second harmonic, n=2, and
$\lambda_u = 0.93\,cm\,,\quad K = 1.5\,,\quad \rho_1^{II} = 1.107\cdot 10^{-3}$ if tuned at the third harmonic, n=3.

The cutting point in the first section is fixed by demanding that the induced energy spread satisfies the condition $\sigma_i(z) \le \frac{\rho_1^I}{2}$.
Accordingly, from eq. 3.11), it can be obtained

$$Z_c \cong 0.94 Z_{F,1}^I - 2 L_{g,1}^I \left[1.22 + ln\left(\frac{\rho_1^I}{\rho_1^{II}} \right) \right] \qquad 3.36)$$

The growth of the field P_1^{II} in the second section is reproduced by

$$P_1^{II}(z) = P_b \frac{H(z)}{1 + \frac{P_b}{P_{F,1}^{II}} H(z)}, \qquad P_b = \left| b_{1,0}^{II} \right|^2 \frac{\rho_1^{II} P_E}{2}$$
$$H(z) = F(z) + \left[\left(\frac{\rho_1^I}{\rho_1^{II}} \right)^n - 1 \right] B(z) \qquad 3.37)$$

where $F(z)$ and $B(z)$ are the functions of eq. 3.33) and eq. 3.24) respectively with the gain length of the second section and n is the order of the harmonic in the first section amplified in the second section.

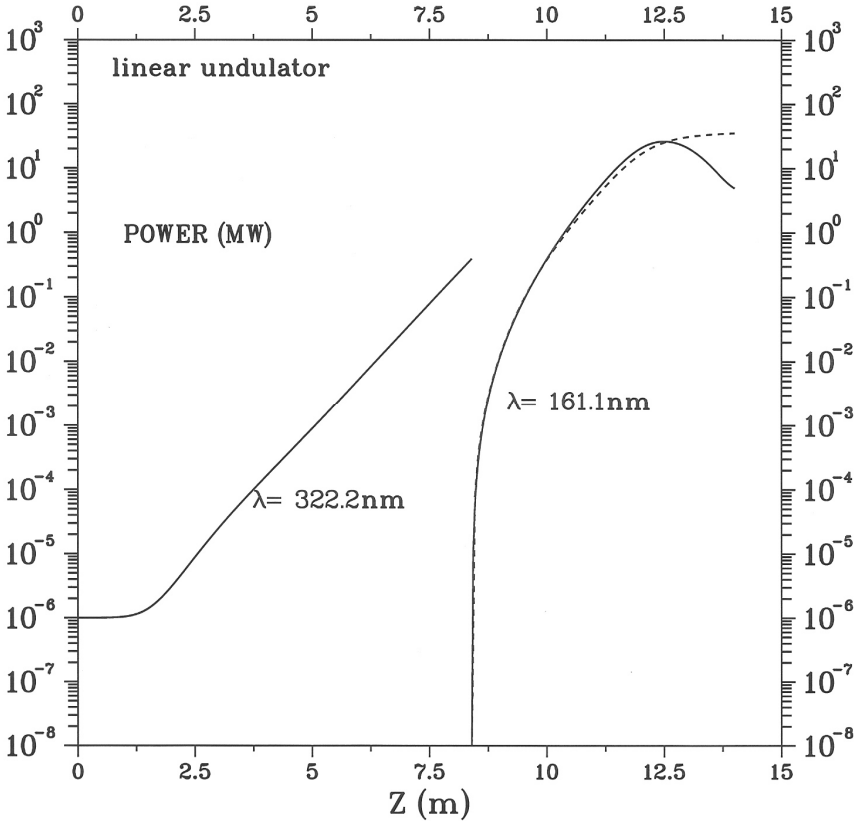

Fig. 3.9 Evolution of the FEL power in a segmented undulator configuration where the 2-nd section is tuned at the 2-nd harmonic of the 1-st section. Continuous line: 1-D simulation, dashed line: eq. 3.37).

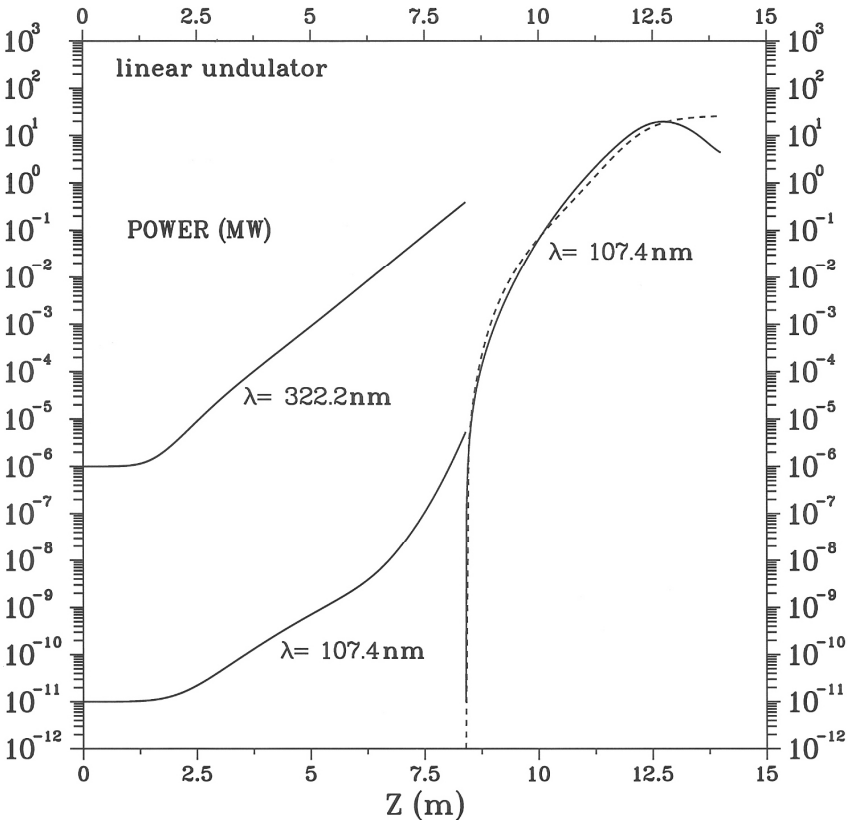

Fig. 3.10 Evolution of the FEL power in a segmented undulator configuration where the 2-nd section is tuned at the 3-rd harmonic of the 1-st section. Continuous line: 1-D simulation, dashed line: eq. 3.37).

The behaviour of the bunching coefficient $|b_1|^2$ in the second section (Figs. 3.11, 3.12) is reproduced by

$$\left|b_1^{II}(z)\right|^2 = \left|b_{1,0}^{II}\right|^2 \frac{L(z)}{1+\left|b_{1,0}^{II}\right|^2\left[L(z)-1\right]}, \qquad L(z) = G'(z) + \left[\left(\frac{\rho_1^I}{\rho_1^{II}}\right)^n - 1\right]B(z) \tag{3.38}$$

$$G'(z) = cosh\left(\frac{z}{L_{g,1}}\right) + \left(\frac{\rho_1^I}{\rho_1^{II}}\right)^2 sin\left(\frac{z}{L_{g,1}}\right) cosh\left(\frac{z}{2L_{g,1}}\right)$$

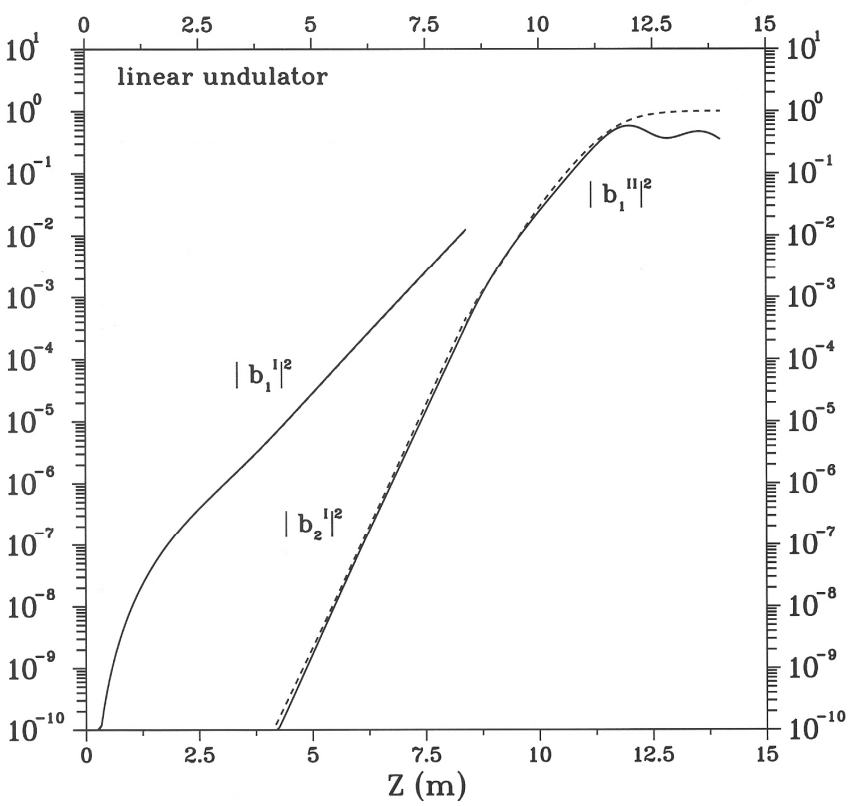

Fig. 3.11 Evolution of the bunching coefficients in a segmented undulator configuration where the 2-nd section is tuned at the 2-nd harmonic of the 1-st section. Continuous line: 1-D simulation, dashed line: eqs. 3.23), 3.24) and 3.38). For $\left|b_1^I\right|^2$ the theoretical formula result exactly overlaps the simulation one.

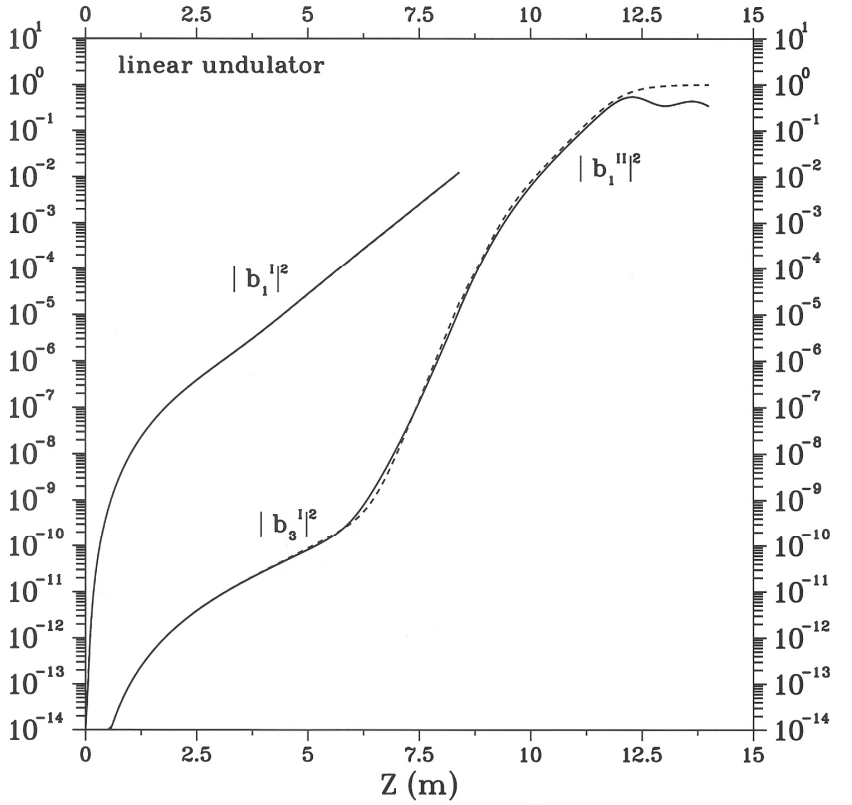

Fig. 3.12 Evolution of the bunching coefficients in a segmented undulator configuration where the 2-nd section is tuned at the 3-th harmonic of the 1-st section. Continuous line: 1-D simulation, dashed line: eqs. 3.24), 3.32) and 3.38).

4 - EXOTIC UNDULATORS

In order to enhance harmonic generation in high gain FEL lasers, non conventional undulator schemes are considered in which the on-axis field oscillates in both transverse directions or in the same direction with different periods. These types of undulators are called bi-harmonic.

4.1 Generalized Bessel Functions

We introduce the generalized Bessel functions which will be used in the FEL equations for bi-harmonic undulator.

$$ {}^{(m)}J_n(x,y) = \frac{1}{\pi}\int_0^{\pi} cos\left[n\vartheta - x\,sin\,\vartheta - y\,sin(n\vartheta)\right]d\vartheta = \sum_{l=-\infty}^{+\infty} J_{n-ml}(x)J_l(y), $$

$$ \sum_{n=-\infty}^{+\infty} e^{in\vartheta}\ {}^{(m)}J_n(x,y) = e^{i\,x\,sin(\vartheta)+i\,y\,sin(m\vartheta)} \qquad 4.1) $$

4.2 Bi-harmonic undulator

We consider here the more interesting case of linear orthogonal polarization with

$$ \vec{B}_u \equiv \left[d\,B_0\,sin(h k_u z), B_0\,sin(k_u z), 0\right] \qquad 4.2) $$

The FEL equations maintain the same structure as eq. 3.1) where now the summation index n runs over both the sets of harmonics with x and y polarization with harmonic numbers n_x and $(hn)_y$ respectively.

The Bessel function factors become

$$ f_{b,n_x} = (-1)^{\frac{n-1}{2}}\left[{}^{(h)}J_{\frac{n-1}{2}}\left(n\xi, (-1)^{h+1}\frac{d^2}{h^2}\left(\frac{n\xi}{h}\right)\right) - {}^{(h)}J_{\frac{n+1}{2}}\left(n\xi, (-1)^{h+1}\frac{d^2}{h^2}\left(\frac{n\xi}{h}\right)\right)\right] $$

$$ f_{b,(hn)_y} = \frac{d}{h}(-1)^{\frac{(n-1)h}{2}}\left[{}^{(h)}J_{\frac{h(n-1)}{2}}\left(hn\xi, (-1)^{h+1}\frac{d^2}{h^2}(n\xi)\right) + (-1)^h\ {}^{(h)}J_{\frac{h(n+1)}{2}}\left(hn\xi, (-1)^{h+1}\frac{d^2}{h^2}(n\xi)\right)\right] $$

with

$$ \xi = \frac{1}{4}\frac{K^2}{1+\frac{K^2}{2}\left(1+\frac{d^2}{h^2}\right)} \qquad 4.3) $$

$$ \lambda_0 = \frac{\lambda_u}{2\gamma^2}\left[1+\frac{K^2}{2}\left(1+\frac{d^2}{h^2}\right)\right] $$

When $d = h = 3$ one obtains the more simple expressions

$$f_{b,1_x} = {}^{(3)}J_0\left(\xi, \frac{\xi}{3}\right) - {}^{(3)}J_1\left(\xi, \frac{\xi}{3}\right)$$

$$f_{b,3_x} = -{}^{(3)}J_1(3\xi, \xi) + {}^{(3)}J_2(3\xi, \xi) \qquad 4.4)$$

$$f_{b,3_y} = {}^{(3)}J_0(3\xi, \xi) - {}^{(3)}J_2(3\xi, \xi)$$

$$\xi = \frac{1}{4}\frac{K^2}{1+K^2}, \qquad \lambda_0 = \frac{1}{2\gamma^2}\left(1+K^2\right)$$

In Fig. 4.1 an example is given of a bi-harmonic power growth 1-D simulation.

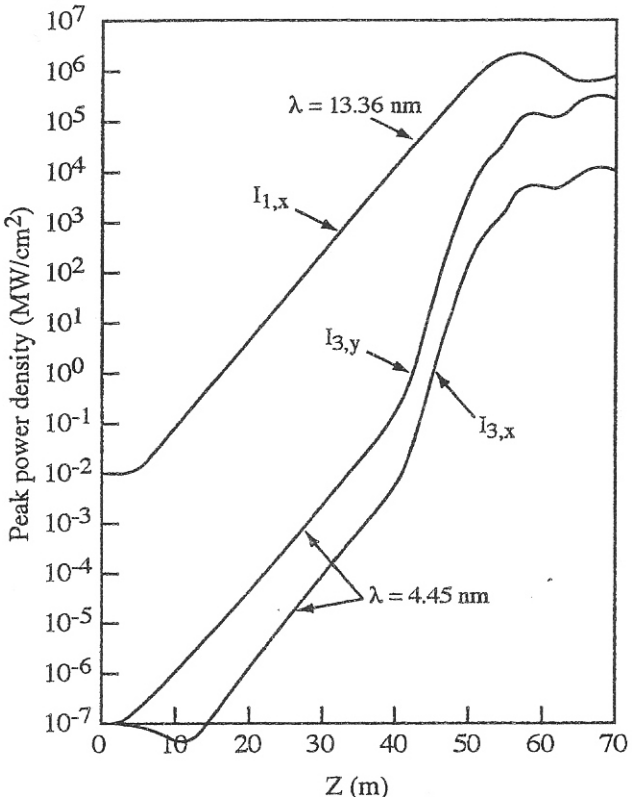

Fig. 4.1 Power growth of main and third harmonics for a bi-harmonic undulator with $d = h = 3$, $E = 1078 Mev$, $\lambda_u = 6\ cm$, $K = 0.99$, $\rho = 1.258 \cdot 10^{-3}$.

5 - PULSE PROPAGATION: HIGH GAIN LINEARLY POLARIZED AMPLIFIER

5.1 Definitions and parameters

In the following we will deal with main harmonic.
A gaussian form is assumed for the e-bunch longitudinal profile

$$f(t) = exp\left[-\frac{1}{2}\left(\frac{t}{\sigma_b} \right)^2 \right]$$

σ_b $\quad e-bunch\ length\ (r.m.s.\ standard\ deviation)$

$\mathcal{P}_F$ $\quad saturated\ peak\ power$ 5.1)

$\mathcal{Z}_F$ $\quad saturation\ length$

$\Delta = \mathcal{N}_F \lambda_0$ $\quad slippage\ length;\qquad \mathcal{N}_F = \mathcal{Z}_F / \lambda_u$

$\mu_c = \dfrac{\Delta}{\sigma_b}$ $\quad longitudinal\ mode\ coupling\ parameter$

For inhomogeneous broadening parameter $\chi \cong 1$ (sects. 3.3, 3.4) $\mathcal{P}_F$ and $\mathcal{Z}_F$ are related to P_F and Z_F of the continuous e-beam case by

$$\mathrm{Z}_F = \left[1 + \exp\left(-3.69\sqrt{\frac{\pi}{\mu_c}} \right) \right] Z_F$$

5.2)

$$\mathrm{P}_F = \left[1 - \exp\left(-1.7\frac{\pi}{\mu_c} \right) \right] P_F$$

5.2 Fundamental harmonic optical packet profile

We derive the optical packet profile from a generalization of the logistic function 3.9)

$$P(z,t) = \frac{P_0(t)}{9} \frac{exp\left(\dfrac{az}{\mathcal{Z}_F} \right) exp\left(\dfrac{z}{L_g(z,t)} \right)}{1 + \dfrac{P_0(t)}{9\mathcal{P}_F}\left[exp\left(\dfrac{z}{L_g(z,t)} \right) - 1 \right]}$$

5.3)

$$L_g(z,t) = \frac{L_g}{g(z,t)}, \qquad g(z,t) = \left[\frac{\mathrm{I}(z,t)}{I(z)} \right]^{\frac{1}{3}},$$

L_g is the gain length of the continuous e-beam case and

$$\mathrm{I}(z,t) = \int_{t-l(z)}^{t} f(t')\,dt' \qquad \textit{for constant input seed } P_0(t),$$

$$l(z) = \frac{z\lambda_0}{\lambda_u\left[1+\dfrac{z\lambda_0}{\pi\lambda_u\sigma_b}f_1(z)\right]}\,, \qquad f_1(z) = \left(\frac{\mathcal{Z}_F}{z}\right)^{\frac{1}{2}}\mathrm{H}(\phi)$$

$$\mathrm{H}(\phi) = c_1\frac{exp[(\phi-c_2)/c_3]}{1+exp[(\phi-c_2)/c_3]} + c_4\phi^{\frac{1}{\sqrt{3}}}\,, \qquad \phi = \frac{\lambda_u\sigma_b}{\lambda_0 L_g} \qquad 5.4)$$

$c_1 \cong 0.62 \qquad c_2 \cong 6.9 \qquad c_3 \cong 0.44 \qquad c_4 \cong 0.43$

The e-bunch is modelled as a set of "slices" of equal length. The core of the SASE pulse dynamics is contained in the integral $\mathrm{I}(z,t)$ which takes into account the number of slices at position t in the e-bunch coupled by the FEL interaction after that the electrons have travelled for a distance z in the undulator.
In order to account for variable or random input signal $P_0(t)$ this integral has to be replaced by the summation

$$\mathrm{I}(z,t) = \sum_{n=1}^{n_s(z)} W(z,t'_n)\, f(t'_n)\Delta t', \qquad t'_n = t - l(z) + n\Delta t' \qquad 5.5)$$

here $\Delta t'$ is the slice length, $n_s(z) = \dfrac{l(z)}{\Delta t'}$ is the "effective" number of coupled slices,

$$W(z,t'_n) = \left(\frac{P_0(t'_n)}{\langle P_0\rangle}\right)^{\frac{1}{n_s(z)+1}}$$

$\langle P_0\rangle$ being the average input signal.

In Figs. 5.1 and 5.2 the evolution of the optical packet at different positions inside the undulator is shown and a comparison is given between numerical 1-D simulations and theoretical formulas. The plots have been normalized to the maximum of the numerical value; the maximum z value correspond to the saturation length $\mathcal{Z}_F$.

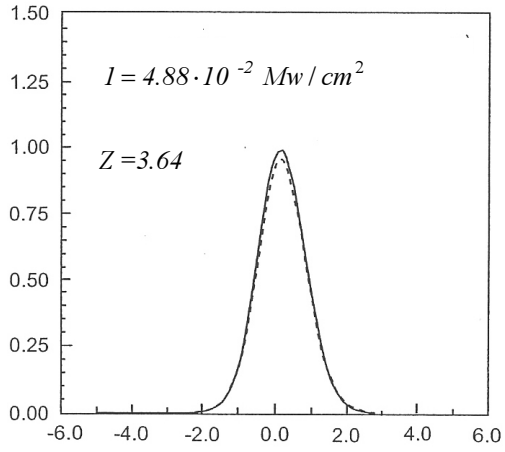

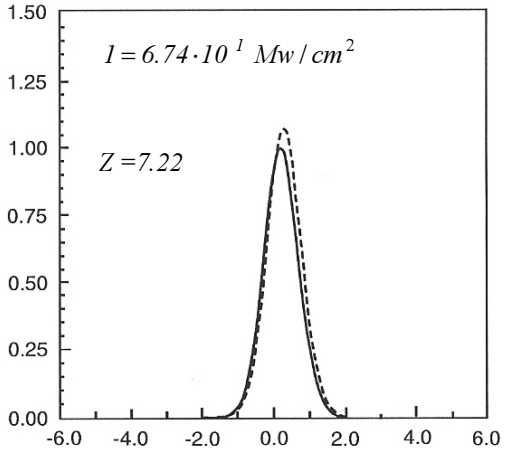

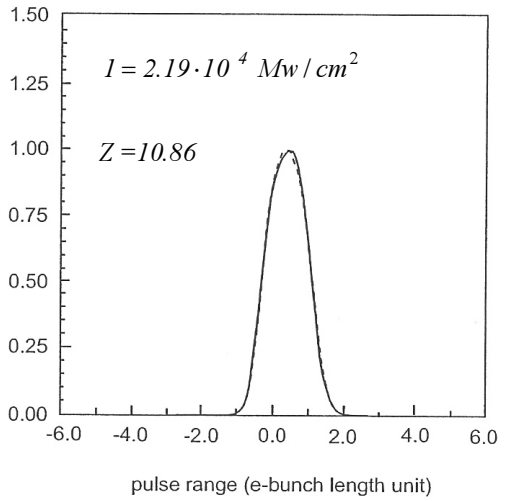

Fig. 5.1 Parameters as in Fig.3.5, $\sigma_b = 96\ \mu m$, $\mu_c = 2.0$, constant seed P_0. Continuous line: 1-D simulation, dashed line: theoretical formulas.

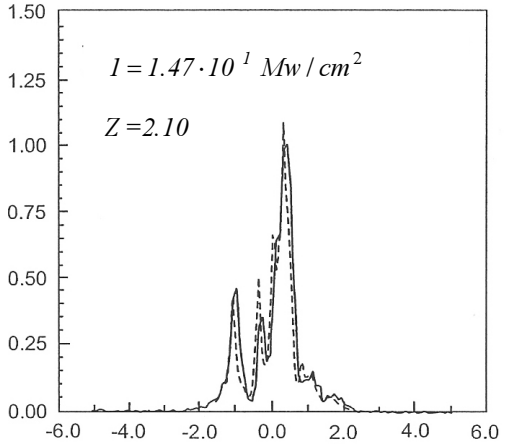

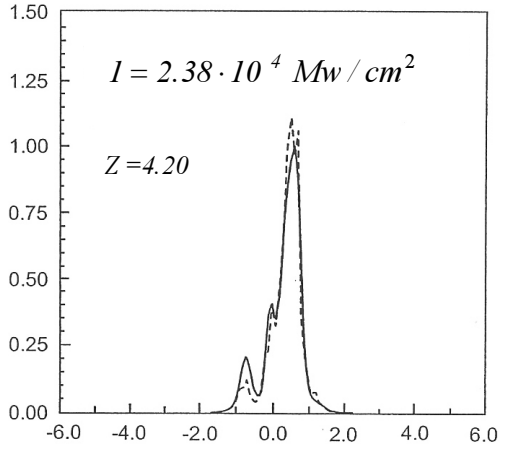

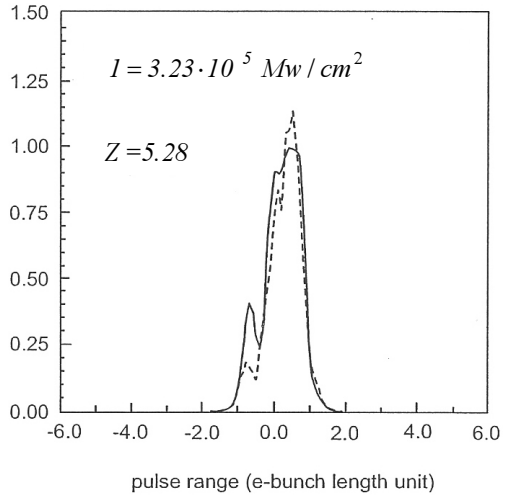

Fig. 5.2 Linear undulator, $E = 156\ Mev$, $\lambda_u = 3.0\ cm$, $K = 1.99$, $\rho = 5.17 \cdot 10^{-3}$, $\sigma_{\varepsilon,0} = 10^{-4}$, $\sigma_b = 96\ \mu m$, $\lambda_0 = 477.8\ nm$, $\mu_c = 0.88$, random seed with $\langle P_0 \rangle$=10W. Continuous line: 1-D simulation, dashed line: theoretical formulas.

6 - FEL OSCILLATORS: THE CONTINUOUS BEAM CASE

In the following we will consider linearly polarized undulator. We will denote the cavity round trip number as r and the cavity total losses as η. Intensity I_r refers to the undulator entry.

6.1 FEL Oscillator rate equation

$$I_{r+1} = (1-\eta)[G(X_r)+1]I_r, \qquad r = 1, 2, \ldots$$
$$G(X_r) \qquad \textit{gain within an undulator passage at round trip r}$$
$$I_1 \equiv I_0 \qquad \textit{input seed power} \qquad 6.1)$$
$$X_r = \frac{I_r}{I_S}$$

where I_S is the saturation intensity accounting for high gain and inhomogeneous broadening effects (see chap.2).

Net gain

$$G_{net}(X_{r+1}) = \frac{I_{r+1} - I_r}{I_r} = (1-\eta)G(X_r) - \eta \qquad 6.2)$$

Theoretical expressions for $G(X_r)$ are

$$G(X_r) = \frac{G_M}{F(X_r)} \qquad 6.3)$$
$$F(X_r) = 1 + a_1 X_r + a_2 X_r^2, \qquad a_1 = 2\left(\sqrt{2}-1\right), \quad a_2 = 3 - 2\sqrt{2}$$

and

$$G(X_r) = G_M \frac{1 - exp(-\beta X_r)}{\beta X_r}, \qquad \beta = 1.0145 \cdot \frac{\pi}{2} \qquad 6.4)$$

where G_M is the maximum gain (see chap.2).

In Fig. 6.1 a comparison is shown for round trip evolution of gain and main harmonic intensity between 1-D simulation and theoretical formulas.

The intra-cavity FEL induced relative energy spread is reproduced by

$$\sigma_i(X_r) \cong \frac{0.433}{N} exp\left[-0.25(\beta X_r) + 0.01(\beta X_r)^2\right] \sqrt{\frac{\beta X_r}{1 - e^{-\beta X_r}} - 1}$$
$$X_r \le 10 \qquad 6.5)$$
$$\sigma_\varepsilon(X_r) = \left[\sigma_{\varepsilon,0}^2 + \sigma_i^2(X_r)\right]^{1/2} \qquad \textit{total energy spread}$$

The equilibrium intra-cavity intensity, obtained from the condition

$$G(X_r) = \frac{\eta}{1-\eta} \qquad 6.6)$$

using eq. 6.2), results

$$I_e = \left(\sqrt{2}+1\right)\left(\sqrt{\frac{1-\eta}{\eta}G_M} - 1\right) I_S \qquad 6.7)$$

Round trips number necessary to reach 10% of the equilibrium intra-cavity intensity (from eq. 6.7)

$$r^* \cong \frac{ln\left(0.1\, I_e / I_0\right)}{ln\left[(1-\eta)\, G_M + 1\right]} \qquad 6.8)$$

6.2 Intracavity power growth and logistic functions

Main harmonic logistic function

$$I_{r+1} = I_0 \frac{\left[(1-\eta)\left(G_M+1\right)\right]^r}{1+\frac{I_0}{I_e}\left\{\left[(1-\eta)\left(G_M+1\right)\right]^r - 1\right\}} \qquad 6.9)$$

which results from rate equation for constant G.
Higher harmonics logistic functions: no intracavity power accumulation

$$I_{n,r+1} = \Pi_{n,0} \frac{\left[(1-\eta)(1+G_M)\right]^{nr}}{1+\frac{\Pi_{n,0}}{I_n^*}\left\{\left[(1-\eta)(1+G)\right]^{nr} - 1\right\}},$$

$$\Pi_{n,0} = (n-1)!\,(n-2))\sqrt{\frac{n-1}{2}}\, g_{0,n} \frac{P_E}{2N}\left(\frac{I_0}{I_S}\right)^n, \qquad 6.10)$$

$$I_n^* = \frac{1}{4}\frac{\sqrt{n}}{n^3}\sqrt{\frac{n-1}{2}}\, g_{0,n} \frac{P_E}{2N}$$

$n = 3, 5, 7$ *harmonic number*

$\Pi_{n,0}$ *harmonic seed power*

I_n^* *maximum harmonic power*

In Fig. 6.2 a comparison is shown for round trip evolution of energy spread and harmonics intensity between 1-D simulation and theoretical formulas.

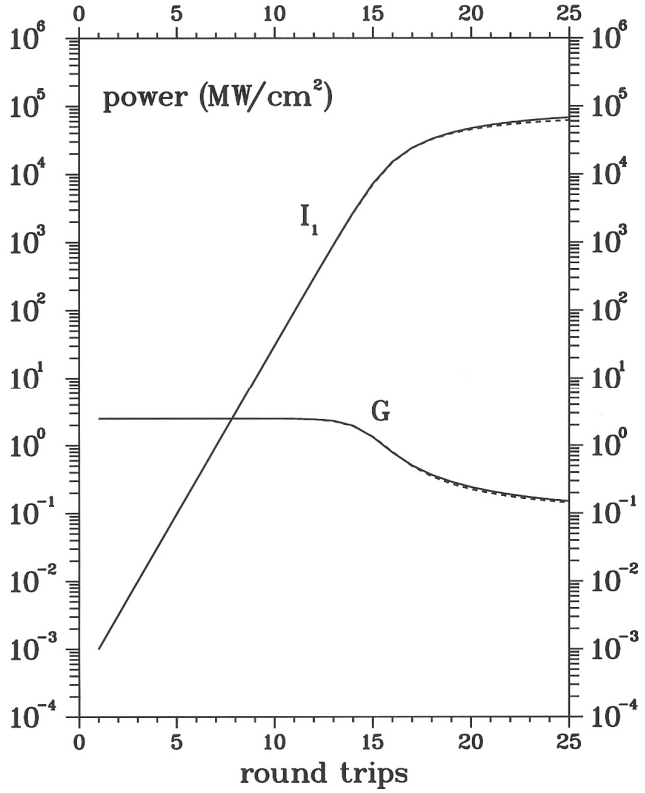

Fig. 6.1 $E = 108.24\,Mev$, $\lambda_u = 2.8\,cm$, $K = 2.10$, $N = 50$, $g_0 = 2.0$, $P_E = 2.012 \cdot 10^6\ MW/cm^2$, $\sigma_{\varepsilon,0} = 10^{-4}$, $I_S = 8.08 \cdot 10^3\ MW/cm^2$, $\lambda_0 = 1.008\,\mu m$, $\eta = 0.10$. Continuous line: 1-D simulation, dashed line: theoretical formulas eqs.6.1), 6.3).

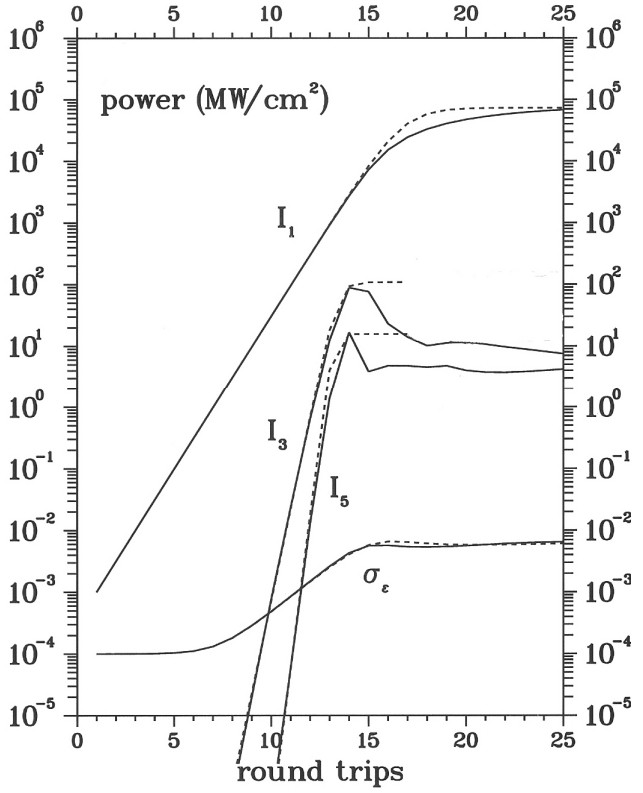

Fig. 6.2 Parameters as in Fig. 6.1. Continuous line: 1-D simulation, dashed line: theoretical formulas eqs.6.5), 6.9), 6.10).

7 – FEL OSCILLATORS PULSED REGIME

In the following we will consider linearly polarized undulator and negligible inhomogeneous broadening effects.

7.1 Parameters (see sect. 5.1)

$$
\begin{aligned}
&\sigma_b && e-bunch\ length\ (r.m.s.\ standard\ deviation)\\
&\Delta = N\lambda_0 && slippage\ \ length\\
&\mu_c = \frac{\Delta}{\sigma_b} && longitudinal\ \ mode\ coupling\ parameter\\
&\delta L && Cavity\ mismatch\ (>0\ for\ cavity\ shortening\ )\\
&\theta = \frac{4\delta L}{g_0 \Delta} && Cavity\ detuning\ parameter\\
&R = \Delta - 2\delta L && Retard
\end{aligned}
\qquad 7.1)
$$

7.2 Low gain (from supermode theory)

Small signal gain including cavity detuning effects - $g_0 \le 0.3$

$$G(\theta,\mu_c) = G_M \frac{\theta}{\theta_s}\left[1 - ln\left(\frac{\theta}{\theta_s}\gamma_c\right)\right], \qquad G_M \cong 0.85 g_0, \qquad \theta_s \cong 0.456$$

$$\gamma_c = 1 + \frac{\mu_c}{3} \qquad 7.2)$$

$$0 \le \theta \le e\frac{\theta_s}{\gamma_c}$$

Maximum gain and corresponding optimum cavity detuning parameter

$$G^* = \frac{G_M}{\gamma_c}, \qquad \theta^* = \frac{\theta_s}{\gamma_c} \qquad 7.3)$$

In the following the definition and notations of chap.6 are used.

Pulsed FEL gain

$$G(X_r,\theta,\mu_c) = G^* \frac{\theta}{\theta^*}\left\{1 - ln\left[\frac{\theta}{\theta^*}F(X_r)\right]\right\} \qquad 7.4)$$

$$X_r = \frac{I_r}{I_S^*}$$

The saturation intensity is denoted by I_S^* because it contains pulse propagation corrections.

Intra cavity equilibrium normalized intensity

$$X_e(\theta,\mu_c) \cong \left(\sqrt{2}+1\right)\left\{\sqrt{\frac{\theta^*}{\theta}}\, exp\left[\frac{1}{2}\left(1-\frac{\eta}{(1-\eta)G^*}\,\frac{\theta^*}{\theta}\right)\right]-1\right\} \qquad 7.5)$$

Intra cavity power logistic function

$$I_{r+1}(\theta,\mu_c) = I_0\,\frac{\left[(1-\eta)\left(G(\theta,\mu_c)+1\right)\right]^r}{1+\frac{I_0}{I_e(\theta,\mu_c)}\left\{\left[(1-\eta)\left(G(\theta,\mu_c)+1\right)\right]^r-1\right\}} \qquad 7.6)$$

Optical Pulse width before saturation at optimum cavity detuning

$$\sigma_E = 0.51\sqrt{\Delta\sigma_b} \qquad 7.7)$$

7.3 High gain correction

Small signal gain including cavity detuning effects

$$G(g_0,\mu_c,\theta) = G^*(g_0,\mu_c)\left[1-\frac{1}{a(\mu_c)}\left(\frac{\theta}{\theta^*(g_0,\mu_c)}-1\right)^2\right] \qquad 7.8)$$

$$a(\mu_c) \cong 5.5\mu_c^{-3/2}$$

with maximum gain

$$G^*(g_0,\mu)_c = \frac{G_M}{1+A(g_0,\mu_c)}, \qquad G_M \ \textit{from eq. 2.1)}$$

$$A(g_0,\mu_c) \cong \frac{\mu_c}{3}+0.074\, exp\left(-1.59\frac{\mu_c}{g_0}\right) \qquad 7.9)$$

and optimum cavity detuning parameter

$$\theta^*(g_0,\mu_c) = \frac{\theta_s}{1+B(g_0,\mu_c)}, \qquad 7.10)$$

$$B(g_0,\mu_c) \cong \frac{\mu_c}{3}+0.38g_0$$

Gain saturation formula

$$G(X_r)=\frac{G^*}{F(X_r)}\left[1-\frac{1}{a}\left(\frac{\theta}{\theta^*}F(X_r)-1\right)^2\right] \qquad 7.11)$$

Intra cavity equilibrium normalized intensity

$$X_E=\left(\sqrt{2}+1\right)\left(\sqrt{Y}-1\right)$$

$$Y=\frac{2\frac{\theta}{\theta^*}-a(\mu_c)\Phi+\sqrt{\left[2\frac{\theta}{\theta^*}-a(\mu_c)\Phi\right]^2+4\left(\frac{\theta}{\theta^*}\right)^2\left[a(\mu_c)-1\right]}}{2\left(\frac{\theta}{\theta^*}\right)^2}, \qquad \Phi=\frac{\eta}{(1-\eta)G^*} \qquad 7.12)$$

The comparison between theoretical formulas and numerical results, shown below, is performed assuming for numerical I_e the average power of the optical pulse. It can be deduced that

$$I_S^*=I_S\cdot\left\{1-exp\left[-\frac{3}{2}\left(\frac{g_0}{\sqrt{\mu_c}}\right)^{1/2}\right]\right\} \qquad 7.13)$$

All figures refer to simulations using:

$\lambda_u=2.8\,cm,\ K=2.10,\ N=50,\ E=108.24\,Mev,\ \lambda_0=1.008\,\mu m$

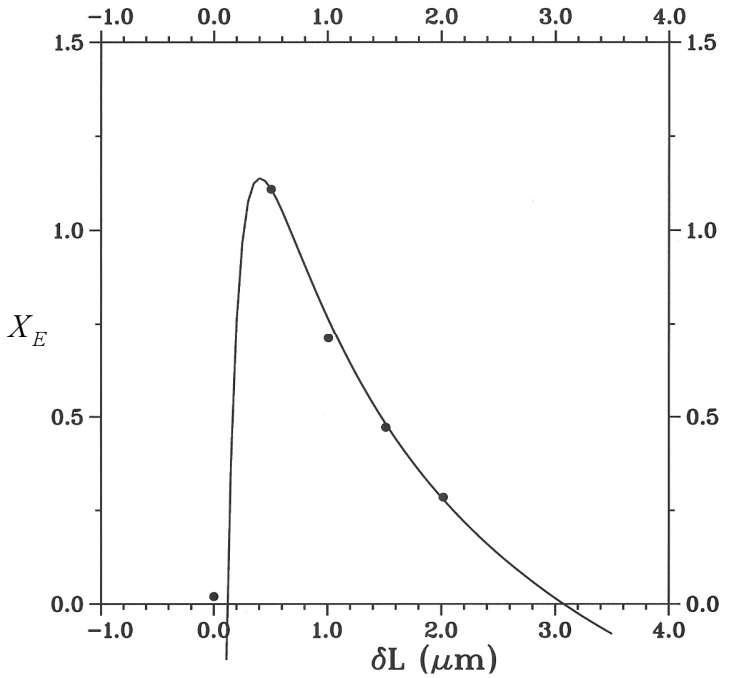

Fig. 7.1 Dimensionless saturated intensity versus cavity mismatch. $g_0=0.3$, $\mu_c=1$, $\eta=0.06$. Continuous line: formula 7.5), dots: numerical results.

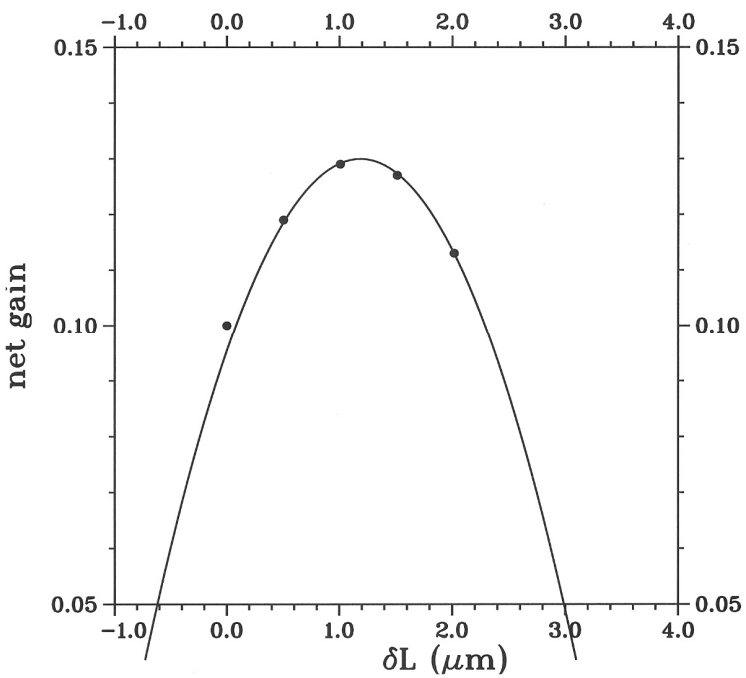

Fig. 7.2 Net gain versus cavity mismatch. Same parameters as in Fig.7.1. Continuous line: formula 7.8), dots: numerical results.

For small g_0 the low gain formula 7.5) well reproduces the saturated power numerical results, while the related gain formula 7.4) does not satisfactory fit the gain numerical results which instead are in good agreement with the general formula 7.8).

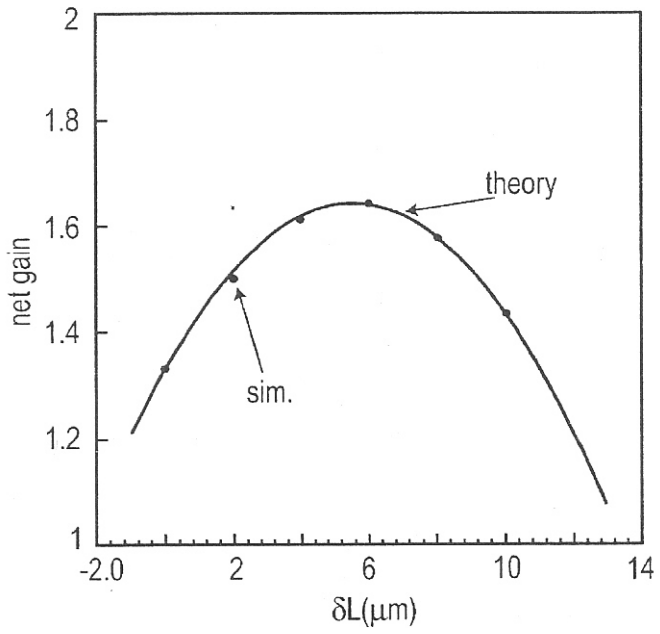

Fig. 7.3 Net gain versus cavity mismatch. $g_0 = 2.0$, $\mu_c = 1$, $\eta = 0.06$. Theoretical results from eq. 7.8).

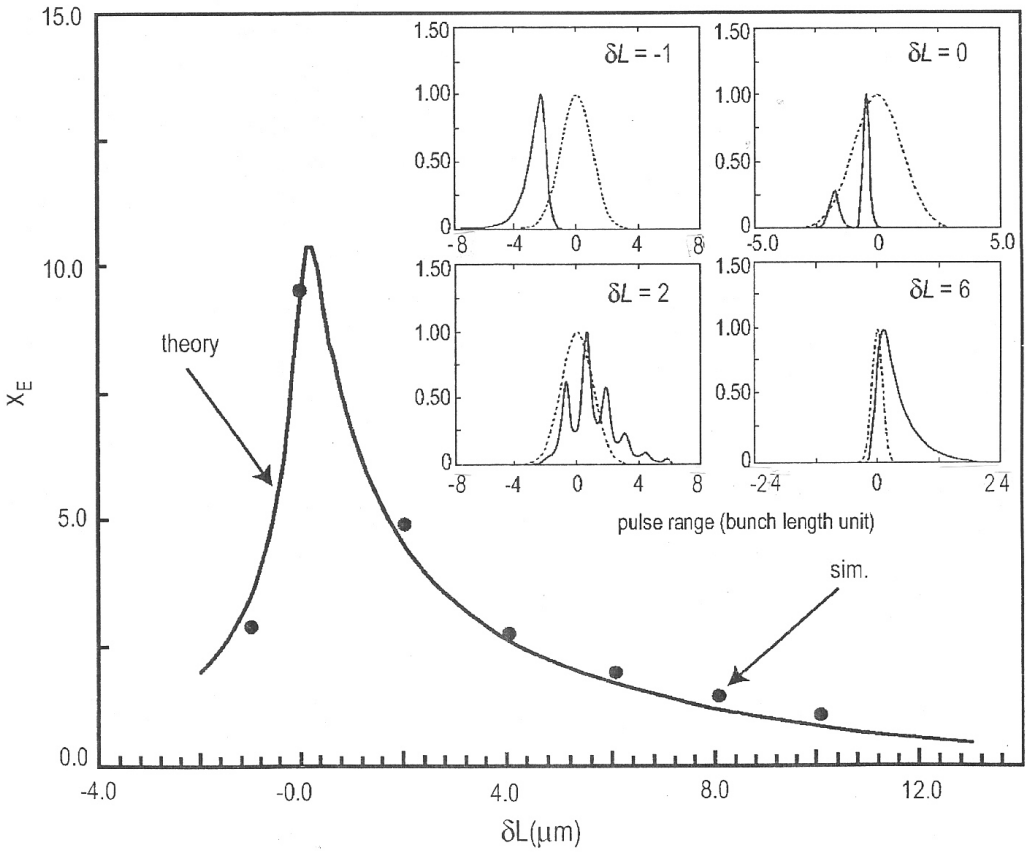

Fig. 7.4 Dimensionless saturated intensity versus cavity mismatch. Same parameters as in Fig.7.3. Theoretical results from eq. 7.12). Shapes of the optical pulses at saturation for different δL values (continuous line), electron bunch (dashed line).

The validity of formulas 7.8) and 7.12) in reproducing the obtained numerical results is limited to a region (or closed to it) of correlated g_0 and μ_c values shown in Fig. 7.5.

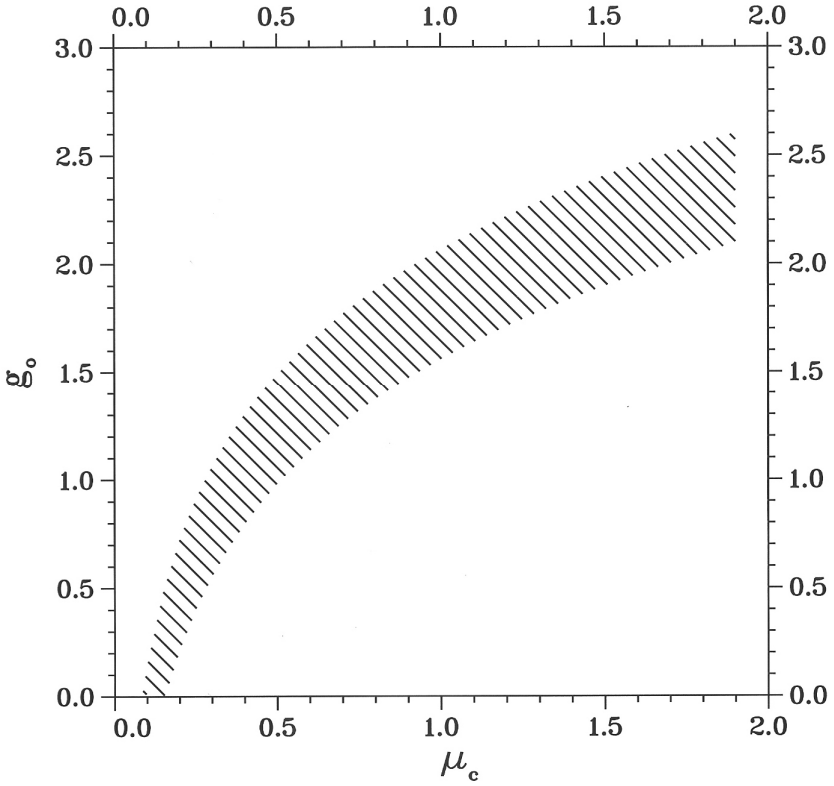

Fig. 7.5 The range of validity of formulas 7.8) and 7.12) is represented by the dashed area in the plane g_0, μ_c.

8 - THE OPTICAL KLYSTRON

The optical klystron (O.K.) is a FEL device characterized by two undulators with the same characteristics (identical polarization, period length and on axis field) separated by a drift section. In the following the small signal gain g_0 and the saturation intensity I_S refer to the single undulator section[8].

8.1 Parameters

$N_1 = N_2 = N$	*Number of periods of the individual undulator section*
N_d	*Number of equivalent periods of the dispersive section*
$\delta = \frac{N_d}{N}$	*Dispersive section parameter*

8.2 **Small signal gain** (no inhomogeneous broadening effects)

Optical klystron gain line shape (Fig. 8.1)

$$G(g_0,\nu,\delta) = -2\pi\, g_0 \frac{d}{d\nu}\left\{\left(\frac{\sin\left(\frac{\nu}{2}\right)}{\frac{\nu}{2}}\right)^2 \left[1+\cos(\nu(1+\delta))\right]\right\} \qquad 8.1)$$

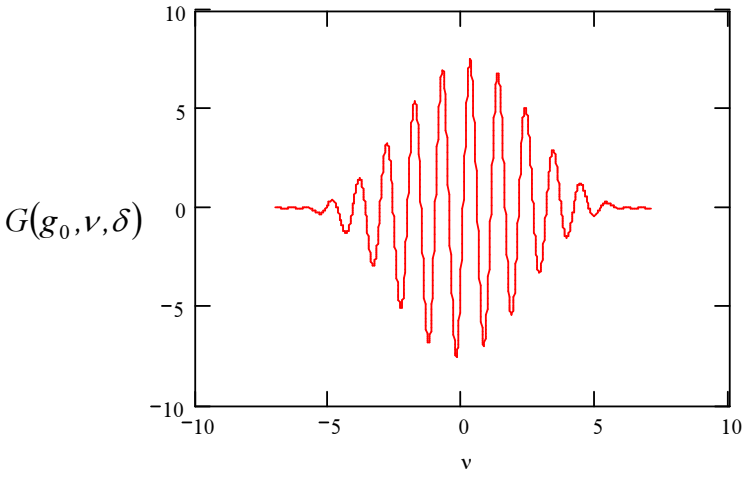

Fig. 8.1 O. K. gain line-shape. $g_0 = 0.2, \delta = 5$

[8] The results of this section are slightly modified with respect to those derived in
G. Dattoli and P. L. Ottaviani IEEE-JQE 35, 27 (1999)
The fitting formulae proposed here have been obtained in such a way that by setting the dispersive section $\delta = 0$ one gets exactly the ordinary FEL formulae. However the equations given in JQE are equally reliable.

Maximum gain

$$G_{M,ok}(\delta) = 0.85\, g_{ok}\ , \qquad g_{ok} = 8 g_0 \left(1 + \frac{p\,\delta^2}{q+\delta} \right) \qquad 8.2)$$

$$p = 0.913,\ q = 0.057$$

Saturation intensity (halving the maximum small signal gain)

$$I_{S,ok}(\delta) = \frac{1.078 \cdot I_{S,2N}}{f(\delta)^2}\ , \qquad I_{S,2N} = \frac{I_S}{16} \qquad 8.3)$$

$$f(\delta) = 1 + \frac{r\,\delta^2}{s+\delta}\ , \qquad r \cong 1.032,\ \ s \cong 0.099$$

8.3 **High gain corrections** (no inhomogeneous broadening effects)

$$G_{M,ok}(g_0, \delta) = 0.85\, g_{ok} + 0.192 \cdot e^{-a\delta} g_{ok}^2 + 4.23 \cdot 10^{-3} \cdot e^{-b\delta} g_{ok}^3 \qquad 8.4)$$

$$a = 2.9 \cdot 10^{-3}\ , \qquad b = 2/3$$

$$I_{S,ok}(g_0, \delta) = \frac{I_{S,ok}(\delta)}{P(8g_0)} exp\left(- \frac{\alpha\, g_0 \delta^3}{1 + \beta\, g_0 \delta^3} \right) \qquad 8.5)$$

$$P(8g_0)\ from\ \ formula\ 2.7)\ \ and\ \ \alpha \cong 1.33 \cdot 10^{-2},\quad \beta \cong 4.41 \cdot 10^{-2}$$

Detuning corresponding to the maximum gain

$$\nu_{M,ok}(g_0, \delta) = \nu_M(8g_0)\, \frac{1}{1 + 0.80\ \delta} \qquad 8.6)$$

where ν_M is from eq. 2.6).

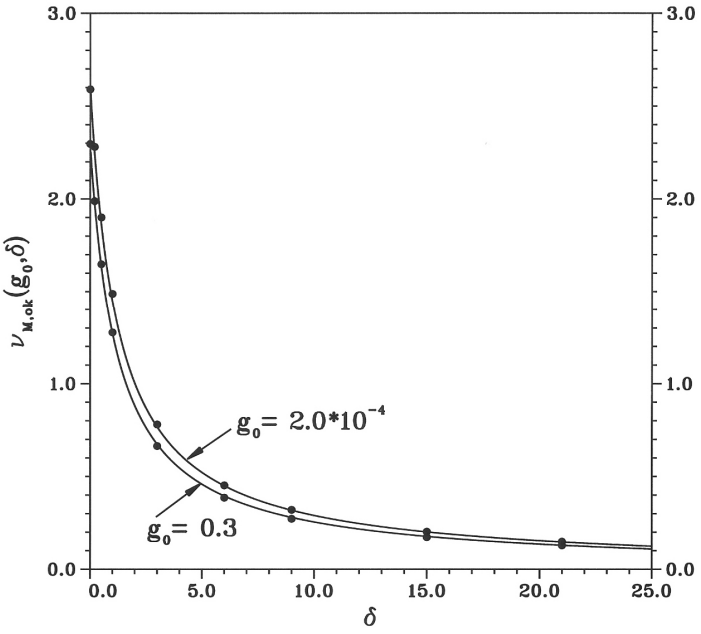

Fig. 8.2 Detuning parameter yielding the maximum gain for O.K. versus δ for two different g_0 values. Solid points: numerical computation; continuous line: eq. 8.6). Relative error < 3%.

The range of validity of the above formulas is $g_0 \le 0.3$, $\delta \le 21$

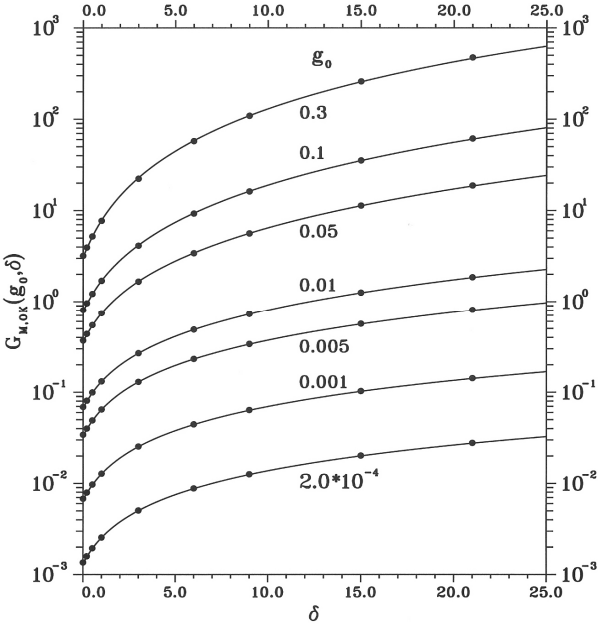

Fig. 8.3 Maximum gain versus δ for different g_0 values. Solid points: numerical computation; continuous line: eq. 8.4). Relative error < 2.5%.

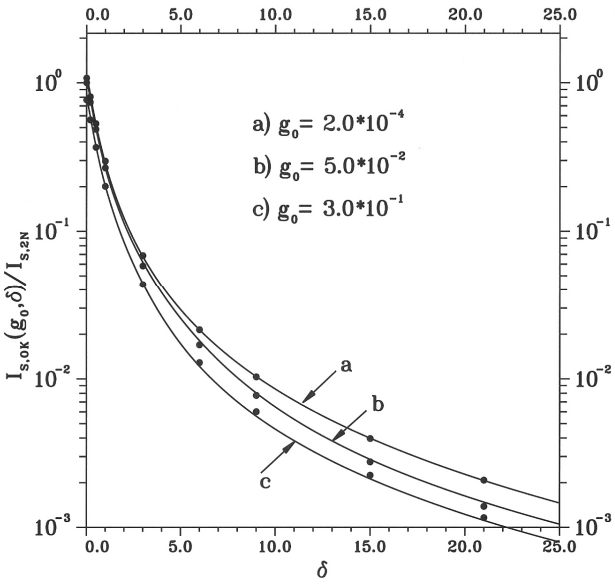

Fig. 8.4 Saturation intensity versus δ for different g_0 values. Solid points: numerical computation; continuous line: eq. 8.5). Relative error < 7 %.

8.4 O. K. gain saturation (no inhomogeneous broadening effects)

$$G_{ok}(g_0,\delta,X) = G_{M,ok}(g_0,\delta)P_{ok}(g_0,\delta,X), \qquad X = \frac{I}{I_{S,ok}(g_0,\delta)}$$

$$P_{ok}(g_0,\delta,X) = \frac{1+Q_{ok}(g_0,\delta)\cdot X(1-X)}{F(X)}$$

$$Q_{ok}(g_0,\delta) = 1 - exp\left[-\frac{a\left(1-bg_0^{1/2}\right)\cdot\delta^{3/2}}{1+c\left(1+dg_0^{1/2}\right)\cdot\delta^{3/2}}\right] \qquad 8.7)$$

$F(X)$ *is defined in eq.* 6.3*) and*

$a \cong 0.193$, $b \cong 0.721$, $c \cong 0.865$, $d \cong 1.346$

valid for $g_0 \le 0.1$, $\delta \le 21$, $X \le 2.5$

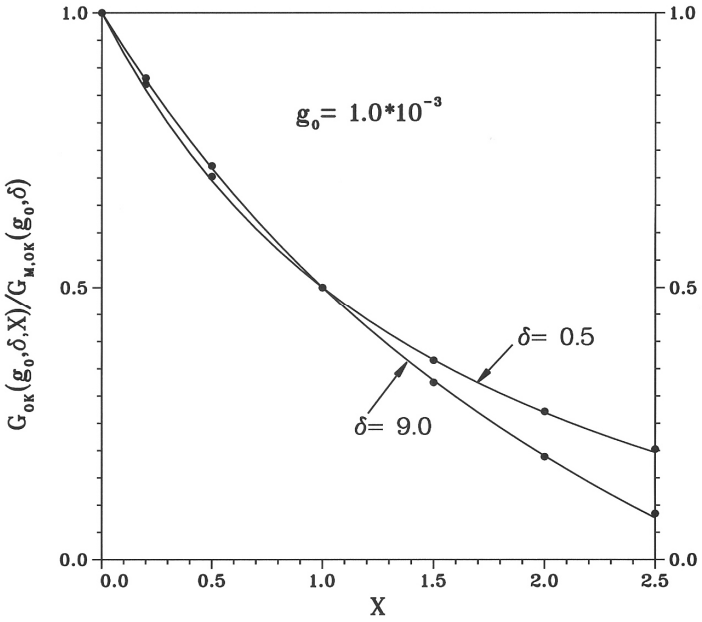

Fig. 8.5a O.K. gain versus X for $g_0 = 10^{-3}$ and two values of δ. Solid points: numerical computation; continuous line: eq. 8.7). Maximum deviation < 9%.

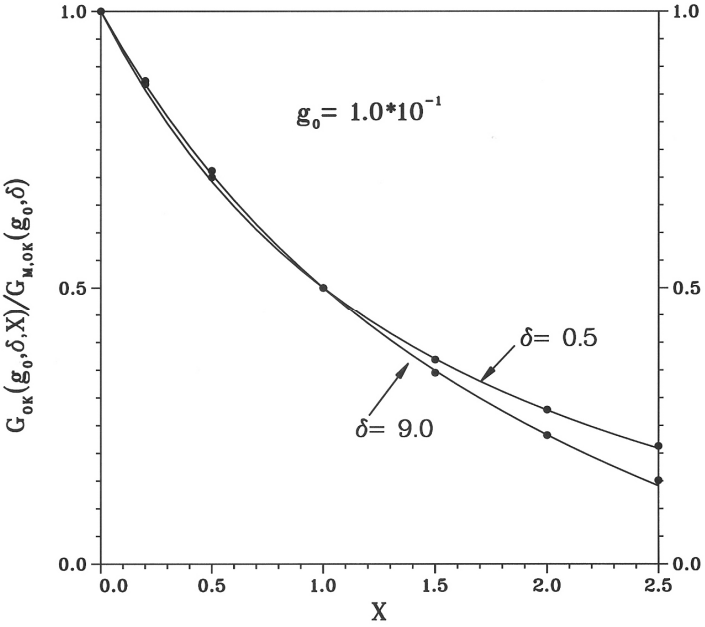

Fig. 8.5b O.K. gain versus X for $g_0 = 0.1$ and two values of δ. Solid points: numerical computation; continuous line: eq. 8.7). Maximum deviation < 7%.

8.5 Energy spread corrections – small signal gain

Inhomogeneous broadening parameters

$$\mu_{ok} = 2\,\mu_\varepsilon(1+\delta), \qquad \mu_\varepsilon = 4N\sigma_\varepsilon \tag{8.8}$$

Gain reduction due to energy spread

$$G_{M,ok}(\delta,\mu_{ok}) = G_{M,ok}(\delta)\,exp\left(-1.228\mu_{ok}^2\right) \tag{8.9}$$

Optimum gain dispersive parameter

$$\delta^* = \frac{1+\mu_\varepsilon^2}{\pi\,\mu_\varepsilon} - 1 \tag{8.10}$$

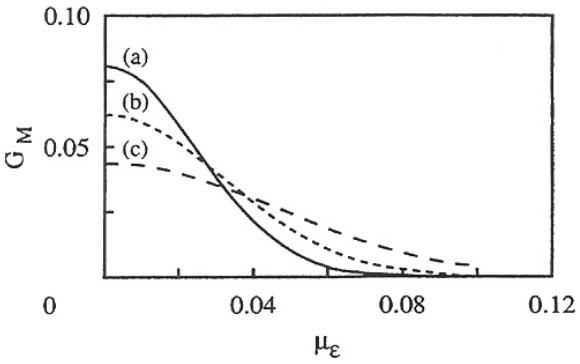

Fig. 8.6 Maximum gain versus μ_ε for $g_0 = 10^{-3}$, $N = 20$ and for different δ values: (a) $\delta = 12$, (b) $\delta = 9$, (c) $\delta = 6$.

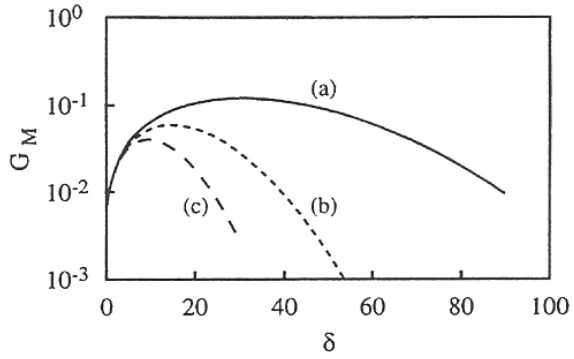

Fig. 8.7 Maximum gain versus δ for $g_0 = 10^{-3}$, $N = 20$ and for different μ_ε values: (a) $\mu_\varepsilon = 10^{-2}$, (b) $\mu_\varepsilon = 2 \cdot 10^{-2}$, (c) $\mu_\varepsilon = 3 \cdot 10^{-2}$.

APPENDIX A

Convolution and inhomogeneous broadening

The effect of the inhomogeneous broadening either on the spontaneous emission or gain can be evaluated by convolving the gain or spontaneous emission line shapes on the energy and/or phase space distribution of the e-beam, thus finding e. g., in the case of the energy distribution $\Phi(\varepsilon)$

$$f_i(\nu) = \int_{-\infty}^{\infty} f(\nu + 4\pi \mathrm{N}\varepsilon)\Phi(\varepsilon)d\varepsilon \qquad \text{A-1)}$$

where the subscript *i* stands for inhomogeneous.
The advantage of using approximations of the spontaneous line shape as given in sec. 1.4 or of the gain as given in eqs. 2.4) is that the integral can be derived in an explicit form.
The effect of the energy spread on the spontaneous emission line shape is indeed provided by

$$f_i(\nu) = \sqrt{\frac{1}{2\alpha\pi^2\mu_\varepsilon^2 + 1}}\, exp\left[-\frac{2\alpha\nu^2 + (\pi\mu_\varepsilon\beta)^2}{2\left(2\alpha\pi^2\mu_\varepsilon^2 + 1\right)} \right] cos\left[\frac{\beta\nu}{2\alpha\pi^2\mu_\varepsilon^2 + 1} \right] \qquad \text{A-2)}$$

APPENDIX B

The small signal limit of the Colson equation (sect. 1.12)

a) Integro-differential form[9]

$$\frac{da}{d\tau} = i\,\pi\, g_0 \int_0^{\tau} \tau'\, e^{-i\nu\tau'} a(\tau-\tau')\, d\tau' \qquad \text{B-1)}$$

b) Operatorial form

$$\begin{aligned} & e^{i\nu\tau}\,\hat{D}_\tau\, a(\tau) = i\,\pi\, g_0\, \hat{D}_\tau^{-2}\left[e^{i\nu\tau}\, a(\tau)\right] \\ & \hat{D}_\tau = \frac{d}{d\tau} \end{aligned} \qquad \text{B-2)}$$

The operator $\hat{D}_\tau^{-n}$ is the negative derivative of n-th order defined as

$$\hat{D}_x^{-n} f(x) = \frac{1}{(n-1)!} \int_0^x (x-\xi)^{n-1} f(\xi)\, d\xi \qquad \text{B-3)}$$

c) Third order differential equation form

$$\begin{aligned} & \left(\hat{D}_\tau^3 + 2i\nu\hat{D}_\tau^2 - \nu^2\hat{D}_\tau\right) a(\tau) = i\,\pi\, g_0 a(\tau) \\ & a|_{\tau=0} = a_0\,, \quad \hat{D}_\tau\, a|_{\tau=0} = 0\,, \quad \hat{D}_\tau^2\, a|_{\tau=0} = 0 \end{aligned} \qquad \text{B-4)}$$

The solution of the equation B-4 can be obtained using standard means, the derivation of the growth of the small signal FEL amplitude is rather cumbersome, because it involves the solution of a cubic equation, without any simplifying assumption. The explicit form writes[10]

[9] G. Dattoli, A. Renieri and A. Torre "Lectures on Free Electron Laser Theory and Related Topics" World Scientific Singapore (1990).

[10] Eq. B-4 appears also in (8) and in an unpublished note by H. Fang written before 1990.

$$a(\tau)=\frac{a_0}{3(\nu+p+q)}\,e^{-\frac{2}{3}i\nu\tau}\left\{(-\nu+p+q)e^{-\frac{i}{3}(p+q)\tau}+\right.$$

$$\left.+2(2\nu+p+q)\,e^{\frac{i}{6}(p+q)\tau}\left[\cosh\left(\frac{\sqrt{3}}{6}(p-q)\tau\right)+i\frac{\sqrt{3}\,\nu}{p-q}\sinh\left(\frac{\sqrt{3}}{6}(p-q)\tau\right)\right]\right\} \qquad \text{B-5)}$$

$$p=\left[\frac{1}{2}(r+\sqrt{d})\right]^{\frac{1}{3}},\quad q=\left[\frac{1}{2}(r-\sqrt{d})\right]^{\frac{1}{3}}$$

$$r=27\pi g_0-2\nu^3,\quad d=27\pi g_0\left[27\pi g_0-4\nu^3\right]$$

which can be exploited to derive the small signal gain and other quantities of practical interest.

It is worth stressing that in the case of a pre-bunched e-beam the problem can be reduced to the same equation B-4) with only difference in the initial conditions, which for a bunched e-beam operation writes

$$a|_{\tau=0}=a_0,\quad \hat{D}_\tau\,a|_{\tau=0}=-2\pi g_0 b_1,\quad \hat{D}_\tau^2\,a|_{\tau=0}=0 \qquad \text{B-6)}$$

Where b_1 is the bunching coefficient defined as

$$b_1=\frac{1}{2\pi}\int_0^{2\pi}f(\zeta_0)e^{-\zeta_0}d\zeta_0 \qquad \text{B-7)}$$

The high gain FEL small signal equation with the inclusion of inhomogeneous broadening terms can be derived from the integral equation B-1) by performing a convolution on the e-beam energy and phase space distribution (matched beam)[11]. The integral equation modifies as it follows

$$\frac{da}{d\tau}=i\pi g_0\int_0^{\tau}\tau'\,\frac{e^{-i\nu\tau'-\frac{1}{2}(\pi\mu_\varepsilon\tau')^2}}{(1-i\pi\mu_x\tau')(1-i\pi\mu_y\tau')}a(\tau-\tau')\,d\tau' \qquad \text{B-8)}$$

[11] For a non matched beam replace $1-i\pi\mu_\eta\tau'$ with $R_\eta=\sqrt{(1+\alpha_\eta^2)(1-i\pi\mu_\eta\tau')(1-i\pi\mu_{\eta'}\tau')-\alpha_\eta^2}$ which for $\alpha_\eta=0$ reduces to the case reported in the modified integral equation.

A useful operatorial form is[12],[13]

$$\frac{da}{d\tau} = i\pi g_0 \int_0^{\tau} \tau' \, a(\tau - \tau') \, \hat{O} e^{-i\nu\tau'} d\tau$$

B-9)

$$\hat{O} = \frac{e^{\frac{1}{2}(\pi\mu_\varepsilon)\partial_\nu^2}}{(1+\pi\mu_x\partial_\nu)(1+\pi\mu_y\partial_\nu)}$$

which can be exploited to treat the problem using a perturbative expansion.

[12] W. B. Colson, J. C. Gallardo and P. M. Bosco, Phys. Rev. 34 A, 4875 (1986),
G. Dattoli, A. Renieri and A. Torre "Lectures on Free Electron Laser Theory and Related Topics" World Scientific Singapore (1990)

[13] The operator $\hat{O}$ is not commuting with the detuning, we cannot therefore reduce the above equation to an ordinary differential equation, it can always be handled to get useful solutions in terms of Volterra type perturbative series, which yield

$$a_n(\tau) = i\pi g_0 \int_0^{\tau} e^{-i\nu\tau'} a_{n-1}(\tau') \hat{O}(\tau') e^{i\nu\tau'} d\tau'$$

APPENDIX C

Logistic equations (chapter 3)

The logistic equation used in sect. 3.2 to model the power growth, satisfies the following differential equations.

$a = 0$

$$\frac{d}{dz}P_1(z) = \frac{P_1(z)}{L_{g,1}}\left[1 - \frac{P_1(z)}{P_{F,1}}\right] \qquad \text{C-1)}$$

or

$$\frac{d}{dz}T(z) = -\frac{1}{L_{g,1}}\left[T(z) - \frac{1}{P_{F,1}}\right], \qquad T(z) = \frac{1}{P_1(z)} \qquad \text{C-2)}$$

which imply a saturation mechanism of the gain depending on the quadratic power of the laser.

$a \neq 0$

$$\frac{d}{dz}P_1(z) = P_1(z)\left[\frac{a}{Z_{F,1}} + \frac{1}{L_{g,1}}\left(1 - \frac{e^{-a\frac{z}{Z_{F,1}}}}{P_{F,1}}P_1(z)\right)\right] \qquad \text{C-3)}$$

The presence of a non vanishing a does not imply that we are considering a different saturation mechanism (the above form does not guarantee any saturation at large z); this factor has just been added in a phenomenological way to better reproduce the numerical data before that final saturation occurs.

Differential equation for power growth including lethargy (the prime denotes derivative with respect to z)

$$\frac{dP_1}{dz} = \left(\frac{\phi'}{\phi} - \frac{A'}{A}e^{-a\frac{z}{Z_{F,1}}}\frac{P_1}{P_{F,1}}\right)P_1 \qquad \text{C-4)}$$

$$\phi = e^{a\frac{z}{Z_{F,1}}}A(z)$$

where $A(z)$ is given in eq. 3.10)

Differential equation for power growth from an initially bunched beam

$$\frac{dP_1}{dz} = \frac{C'}{C}\left(1 - \frac{P_1(z)}{P_{F,1}}\right)P_1(z)$$
$$C = 2\left[cosh\left(\frac{z}{L_{g,1}}\right) - exp\left(-\frac{z}{2L_{g,1}}\right)cos\left(\frac{\pi}{3} - \frac{\sqrt{3}z}{2L_{g,1}}\right) - exp\left(\frac{z}{2L_{g,1}}\right)cos\left(\frac{\pi}{3} + \frac{\sqrt{3}z}{2L_{g,1}}\right)\right] \quad \text{C-5)}$$

The previous logistic equations take into account the fast growing root only; more in general the FEL power density evolution can be written as

$$|A|^2 = \frac{|a(\tau)|^2}{1 + \frac{|a_0|^2}{|A_F|^2}\left[\left|\frac{a(\tau)}{a_0}\right|^2 - 1\right]} \quad \text{C-6)}$$

where $a(\tau)$ is the small signal FEL complex amplitude given in eq. B-5), and $|A_F|^2$ is the dimensionless field saturated intensity defined as

$$|A_F|^2 = 16\sqrt{2}\,\pi^2 g_0 N \rho \quad \text{C-7)}$$